Orally-bioavailable CDK9/2 inhibitor shows mechanism-based therapeutic potential in MYCN-driven neuroblastoma.

Evon Poon[1,2t], Tong Liang[3t], Yann Jamin[4t], Susanne Walz[5], Colin Kwok[1,2], Anne Hakkert[1,2], Karen Barker[1,2], Zuzanna Urban[1,2], Khin Thway[6], Rhamy Zeid[7], Albert Hallsworth[1,2], Gary Box[2,8], Marli E. Ebus[9], Marco P. Licciardello[2,8], Yordan Sbirkov[1,2], Glori Lazaro[2], Elizabeth Calton[1,2], Barbara M. Costa[1,2], Melanie Valenti[2,8], Alexis De Haven Brandon[2,8], Hannah Webber[1,2], Nicolas Tardif[1,2], Gilberto S. Almeida[1,2,4], Rossitza Christova[1], Gunther Boysen[1], Mark W. Richards[10], Giuseppe Barone[1,2], Anthony Ford[6], Richard Bayliss[10], Paul A. Clarke[2,8], Johann De Bono[1], Nathanael S. Gray[11,12], Julian Blagg[2,8], Simon P. Robinson[4], Suzanne A. Eccles[2,8], Daniella Zheleva[13], James E. Bradner[12,14,15], Jan Molenaar[9], Igor Vivanco[2], Martin Eilers[16], Paul Workman[2,8], Charles Y. Lin[3,17*], Louis Chesler[1,2*]

*Co-corresponding authors.

[t] These authors contributed equally to this work.

Affiliations:

Division of [1]Clinical Studies, [2]Cancer Therapeutics, The Institute of Cancer Research, London and The Royal Marsden NHS Trust, Sutton, SM2 5NG, UK.

[3]Baylor College of Medicine, Department of Molecular and Human Genetics, Houston, TX.

[4]Radiotherapy and Imaging, The Institute of Cancer Research, London, SM2 5NG, UK.

[5]Core Unit Bioinformatics, Comprehensive Cancer Center Mainfranken and Theodor Boveri Institute, Biocenter, University of Wurzburg, Am Hubland, 97074 Wurzburg, Germany

[6]Molecular Pathology, The Institute of Cancer Research, London, SM2 5NG, UK.

[7]Dana-Farber Cancer Institute, Department of Medical Oncology, Boston, MA.

[8]Cancer Research UK, Cancer Therapeutics Unit, The Institute of Cancer Research, London, SM2 5NG, UK.

[9]Prinses Maxima Center for Pediatric Oncology, 3584 EA Utrecht, The Netherlands.

[10]School of Molecular and Cellular Biology, Faculty of Biological Sciences, University of Leeds, Leeds LS2 9JT, UK

[11]Department of Cancer Biology, Dana-Farber Cancer Institute, Boston, MA

[12]Department of Biological Chemistry and Molecular Pharmacology, Harvard Medical School, Boston, MA

[13]Cyclacel Ltd., Dundee, United Kingdom.

[14]Department of Medicine, Harvard Medical School, Boston, MA.

[15]Present address: Novartis Institute for Biomedical Research, Cambridge, MA

[16]Comprehensive Cancer Center Mainfranken and Theodor Boveri Institute, Biocenter, University of Wurzburg, Am Hubland, 97074 Wurzburg, Germany.

[17]Present address: Kronos Bio, Cambridge, MA

Address correspondence to:

Louis Chesler, Division of Clinical Studies, The Institute of Cancer Research, London and The Royal Marsden NHS Trust, 15 Cotswold Rd, Sutton, SM2 5NG, UK. Phone: +44(0)2034376122; Email: louis.chesler@icr.ac.uk

Charles Y. Lin, Kronos Bio, Cambridge, MA, U.S.A. Phone: +1-6172764723 ; Email: Charles.y.lin@bcm.edu

Conflict of Interest:

E.P., Y.J., C.K., K.B., A.H., G.B., M.P.L., G.L., B.M.C, M.V., A.D.H.B., H.W., G.A., R.C., G.B., A.F., J.B., P.A.C., J.D.B., S.P.R., S.A.E., P.W., I.V., and L.C., are employees of ICR which has a Rewards to Inventors scheme and has a commercial interest in the development of inhibitors of CDKs, with intellectual property licensed to, and research funding provided by Merck and Cyclacel Pharmaceuticals. C.Y.L. has equity in and intellectual property licensed to Syros Pharmaceuticals. T.L and C.Y.L have equity in Kronos Bio, Inc. P.W. is or has been a consultant/scientific advisory board member for Cyclacel, Astex Pharmaceuticals, CV6 Therapeutics, Nuevolution and Nextechinvest; received grant funding from Cyclacel; is a non-executive director of Storm Therapeutics; and holds equity in Chroma Therapeutics, Nextech and Storm. D.Z. is an employee of Cyclacel Ltd. J.B. holds equity in Neophore Ltd and in Azeria Therapeutics. All other authors declare that they have no conflict of interest regarding the content and publication of this article.

Abstract

The undruggable nature of oncogenic Myc transcription factors poses a therapeutic challenge in neuroblastoma, a paediatric cancer in which *MYCN* amplification is strongly associated with unfavorable outcome. Here, we showed that CYC065 (fadraciclib), a clinical inhibitor of CDK9 and CDK2, selectively targeted *MYCN*-amplified neuroblastoma via multiple mechanisms. CDK9 — a component of the transcription elongation complex P-TEFb — bound to the *MYCN*-amplicon super-enhancer and its inhibition resulted in selective loss of nascent *MYCN* transcription. MYCN loss led to growth arrest, sensitizing cells for apoptosis following CDK2 inhibition. In *MYCN*-amplified neuroblastoma, MYCN invaded active enhancers driving a transcriptionally encoded adrenergic gene expression program that was selectively reversed by CYC065. MYCN overexpression in mesenchymal neuroblastoma was sufficient to induce adrenergic identity and sensitize cells to CYC065. CYC065 used together with temozolomide, a reference therapy for relapsed neuroblastoma, caused long-term suppression of neuroblastoma growth in vivo, highlighting the clinical potential of CDK9/2 inhibition in the treatment of *MYCN*-amplified neuroblastoma.

Introduction:

The prominent role of Myc-family proto-oncogene transcription factors (*MYC*, *MYCN, MYCL)* in the genesis of adult and childhood cancers makes these transcription factors (TFs) attractive targets for drug discovery and development(1). However, the intrinsically disordered structure of Myc proteins, and an incomplete understanding of how Myc, a master regulator of the transcriptomic and epigenetic landscape, co-opts oncogenesis to drive cellular transformation, are two major issues that impede traditional drug discovery approaches(1).

Across many cancers, a singular feature of oncogenic Myc activity is an increase in the abundance of its full length protein(2). This suggests that Myc protein dosage itself is transforming. Strategies to attenuate Myc levels may be sufficient to achieve a therapeutic index in tumors versus normal tissues by selectively targeting oncogenic programmes rather than tissue maintenance programmes where Myc regulates homeostatic ribosome biogenesis and cellular proliferation(3, 4). In both normal and tumor cells, Myc functions primarily as an activator of transcription. When bound to DNA, Myc increases proximal chromatin accessibility via recruitment of histone acetyltransferases(5) and drives transcription elongation through recruitment of the elongation factor P-TEFb (cyclinT1:CDK9)(6) and RNA Polymerase II (RNAPII) associated topoisomerases(7). When deregulated, a consensus has emerged that Myc proteins act as selective amplifiers of gene expression(8, 9). Although Myc deregulation leads to a global increase in cellular mRNA in an oncogenic context, transformation driven by Myc in neuroblastoma (NB), a developmental tumor of neural crest origin, is associated with selective (and enhancer dependent) upregulation of a limited set of lineage-related genes, expression of which normally constitutes a transcriptomic core-regulatory circuit that underlies neural identity and deregulation of which drives growth and proliferation of these tumors(10-12).

We and others have found that MYCN globally upregulates and reshapes the NB gene expression landscape through the invasion of tissue-specific active enhancers that establish NB identity(13). In particular, large super-enhancers which are adjacent to several TFs that demarcate the recently described adrenergic state of NB, exhibit strong MYCN binding and are selectively regulated by MYCN(13). Expression of these TFs, including *GATA3*, *PHOX2A, PHOX2B, HAND2/TWIST1, TBX2* and *ISL1,* is

essential in *MYCN*-amplified NB(11, 13) suggesting that an oncogenic feed-forward interaction between MYCN, tissue-specific enhancers, and additional TFs constitute a core regulatory circuitry that underlies maintenance of lineage-related NB gene-expression programs.

In *MYCN*-amplified NB, the expression of *MYCN* itself is regulated by large super-enhancers that maps to the *MYCN* amplicon(13). This has spurred renewed efforts to target MYCN transcription through inhibition of transcriptional co-regulators that are enriched at enhancers and super-enhancers, including the BET-bromodomain transcriptional co-activators and some of the transcriptional cyclin-dependent kinases (CDK7/9/12/13)(14-18). In NB and other cancers, targeting these transcriptional components leads to selective downregulation of super-enhancer associated genes such as *MYC* or *MYCN* that are characterized by high transcription levels and rapid turnover of RNA. These observations have spurred further pre-clinical investigation of transcriptional inhibition in NB. However, as almost all cells have super-enhancers at key identity genes, it remains unclear how transcriptional inhibition can achieve selectivity, how Myc addiction is subverted by transcriptional inhibition to kill tumor cells, and how a therapeutic strategy for transcriptional inhibition can be implemented.

Here in order to accelerate the clinical implementation of transcriptional inhibitors in NB, we investigate the ability of CYC065 (fadraciclib), a selective inhibitor of CDK9 and CDK2 that has reached clinical early-phase trials, to selectively target *MYCN*-amplified tumors via multiple mechanisms. CYC065(19) and its analogue CCT068127(20) were discovered in a research programme aimed at identifying derivatives of seliciclib(21) with greater potency, solubility and metabolic stability(22).

Results:

CDK9 inhibition downregulates MYCN and is selective against *MYCN*-amplified NB.

We evaluated a series of clinical candidate drugs and toolkit compounds with potent and selective activity against CDK9 and varying activity against other CDKs. We observed that compounds with prominent activity against CDK9 are efficient in downregulating MYCN to varying degrees and inducing apoptotic cell death as indicated by induction of PARP cleavage (Supplemental Figure 1A, 2B). Of these compounds, we

selected the chemical probe CCT68127(22), and its further optimized derivative CYC065 that is in early phase clinical trials — both with significant selectivity for CDK9/2(20, 23) (Supplemental Figure 2A-B). We evaluated CYC065 and CCT68127 across a set of NB cell lines (Figure 1A; Supplemental Figure 2D,E) varying in *MYCN* amplification and protein levels and characterized for MYCN or MYC dependence(15). MYCN-driven cell lines exhibited time- and concentration-dependent growth inhibition, increased cell death (by sub G1 population) and induction of apoptosis (caspase-3 and PARP cleavage), resulting in loss of cell viability and with prolonged treatment, blockade of colony-formation (Figure 1B-E; Supplemental Figure 2C,E-H). These effects occurred at concentrations of CYC065 and CCT68127 coinciding with a reduction in MYCN protein, and a reduction in phosphorylation of RNAPII Serine 2 (RNAPII Ser2P), a canonical substrate of CDK9 (Figure1C; Supplemental Figure 2H). Notably, in non-*MYCN*-amplified NB (SH-EP, SH-SY5Y and SK-N-AS cells), CYC065 still potently reduced RNAPII Ser2P at compound concentrations that have no or little impact on apoptosis (Supplemental Figure 2I,J) suggesting that transcriptional inhibition is not lethal in these non-*MYCN*-amplified cells.

At the cellular GI50, a concentration at which cell growth is inhibited by 50%, CYC065 and CCT68127 primarily cause cell growth arrest and apoptosis in *MYCN*-amplified NB cells (Figure1A-B; Supplemental Figure 2D-F). Contrary to prior reports in lung cancer cells that CCT68127 caused anaphase catastrophe(18), NB cells treated with CYC065 at low concentrations exhibited intact mitotic spindle formation, and at higher concentrations or with prolonged treatment exhibit DNA fragmentation consistent with apoptosis (Supplemental Figure 3A). These data suggested that at concentrations close to the GI50, and therefore relevant to the mechanism of action for CDK9 and 2, CYC065 treatment results in growth arrest and apoptosis in *MYCN*-amplified cells.

Cell-death upon CDK9-inhibition is enhanced by concomitant blockade of CDK2 activity.

We observed that in comparison to mono-selective inhibitors of CDK9, such as Compound 3, which is able to induce PARP cleavage at high concentrations, CYC065 caused a high level of apoptotic cell death at cellular GI50 concentrations in *MYCN*-amplified NB cells, presumably due to concomitant inhibition of CDK2, itself a major regulator of apoptotic cell death. Apoptosis occurred concomitant with a marked reduction in MCL-1 (Supplemental Figure 1A, 2H), a transcriptional target of CDK9 with prominent pro-

survival activity dependent on CDK2 phosphorylation(24). Using a fluorescence-based cellular sensor that measures phosphorylation of substrate by CDK2(25), we confirmed that at the GI50 concentration, CYC065 reduced CDK2-driven kinase activity (Figure 2A), blocked phosphorylation of Histone H1 (a direct substrate of CDK2, Figure 2B) and upregulated the pro-apoptotic CDK2 targets (Supplemental Figure 4A). In contrast, NVP-2, a highly potent and selective CDK9-only inhibitor failed to decrease CDK2 substrate phosphorylation to the same degree (Figure 2a).

With extended exposure to CYC065 (8hr), we also observed a reduction in phosphorylation of Rb Serine 780 (Figure 2C), and an accumulation of total and phosphorylated p53 (Supplemental Figure 2H, 4B-D, 5H), both known consequences of CDK2 inhibition(15). In CDK9-inhibited and MYCN-dependent cells, activation of apoptotic cell-death is CDK2-dependent, as the mono-selective CDK9 chemical probe (Compound 3)(26), the clinical mono-selective CDK9 inhibitor BAY1143572(27) (atuveciclib) and knockdown of CDK2 with siRNA each failed to induce robust apoptosis (Figure 2D, Supplemental Figure 4E, 4G). In contrast to mono-specific inhibition of CDK9 or CDK2, the combination of selective CDK9 inhibition (Compound 3 or BAY1143572) with siRNAs directed at CDK2 resulted in enhanced PARP cleavage (Figure 2D; Supplemental Figure 4E, 4G). Since the siRNA knockdown of CDK2 is modest, we performed CRISPR Cas9-mediated knockout of CDK2 in *MYCN*-amplified Kelly cells (Supplemental Figure 5G), which elicited minimal effects on apoptosis or cell cycle distribution (Supplemental Figure 4G), and in parental *MYCN*-amplified Kelly cells, selective chemical inhibition or genetic knockdown of CDK9 or CDK2 alone failed to phenocopy the growth inhibitory effects of CYC065 (Figure 2E; Supplemental Figure 4G). Finally, we observed that only in CDK2 knockout cells, did Compound 3 treatment or CDK9 degradation using THAL-SNS-032(28) (a potent and selective CDK9 degrading PROTAC) result in an increase in subG1 apoptotic cells (Supplemental Figure 4F-G) and growth inhibitory effects (Figure 2E). Taken together these data confirm that in the setting of CDK9-induced MYCN blockade, activation of apoptotic cell-death in *MYCN*-amplified NB requires concomitant diminution of CDK2 activity.

CDK9 inhibition blocks nascent transcription of *MYCN* and other highly transcribed genes.

Together with cyclin T1, CDK9 forms P-TEFb, which promotes transcriptional elongation via direct phosphorylation of Ser2 in the carboxy-terminal repeat (CTD) of RNAPII(29-33). Consistent with its property

to inhibit CDK9, CYC065 at GI50 concentration blocked phosphorylation of RNAPII Ser2, while RNAPII Ser5, a target of CDK7, was inhibited only at higher concentrations (Supplemental Figure 1A, Figure 3A-B). Short-term treatment (1hr) with CYC065 or CCT68127 globally reduced, but did not totally block, nascent RNA synthesis as determined by *in situ* staining (Figure 3C-D). In comparison, Actinomycin D (ActD), which inhibits transcription initiation, completely abrogated nascent transcription at a 0.5 µg/ml concentration. These results suggest that CDK9 inhibition at least partially inhibits global transcription elongation.

Using high resolution imaging, we noticed consistent overlap of nascent transcription foci at the *MYCN* amplicon (visualized by DNA FISH) that were abrogated by the exposure to the GI50 concentration of CYC065 (Figure 3E). Loss of *MYCN* transcript temporally coincided with global loss of nascent transcription and chromatin acetylation as evidenced by H3K27ac levels (Figure 3F). This is consistent with the overall role of Myc proteins in amplifying gene expression(8, 9) and maintaining open chromatin(34). Indeed, nascent transcription of highly expressed, high turnover transcripts like *MYCN* and *MCL-1* is almost completely inhibited within 15 minutes of CYC065 treatment (Figure 3G), and overall, short half-life genes like *MYCN* (Supplemental Figure 5A) are selectively depleted from the cellular mRNA pool (Figure 3H). In contrast, CYC065 had only modest effect on MYCN protein turnover (Supplemental Figure 5B-C). MYCN loss was phenocopied by selective degradation of CDK9 by THAL-SNS-032 and genetic depletion of CDK9 or to a lesser extent CDK7 (Supplemental Figure 5D-F), consistent with a general sensitivity of *MYCN* to transcriptional inhibition. Knockdown of CDK2 did not affect MYCN levels (Figure 2D, Supplemental Figure 4F, 5G). Notably, when MYCN was exogenously expressed, its levels were no longer sensitive to CYC065 or CCT68127 (Supplemental Figure 5H). These data confirm that nascent transcription of the *MYCN* amplicon is uniquely sensitive to transcriptional perturbation, and to inhibition of CDK9.

Further analysis of mRNA levels upon CYC065 treatment across a panel of *MYCN*-amplified NB cell lines as well as tumors from the MYCN-driven TH-*MYCN* mouse model revealed a selective depletion of Myc target gene expression (Figure 3I, Supplemental Figure 6E). This effect was confirmed at individual genes, on a Myc target luciferase reporter, and by showing depletion of MYCN from a target gene promoter by ChIP (Supplemental Figure 5A,I-J). Although MYCN depletion was much more pronounced in *MYCN*-amplified NB (Supplemental Figure 6B), depletion of Myc-driven house-keeping gene expression was also

consistently observed in non-*MYCN*-amplified NB (Figure 3I, Supplemental Figure 6A-E), suggesting that irrespective of *MYCN* amplification status, CDK9 inhibition targets canonical Myc target gene signatures associated with growth and biogenesis.

MYCN enhancer invasion shapes NB-specific responses to CYC065.

Although CYC065 downregulated canonical Myc target gene expression in both *MYCN* and non-*MYCN*-amplified NB, its highly-selective effects on *MYCN*-amplified NB growth spurred us to further investigate why and how MYCN expression or amplification induces this dependency in NB. We considered two hypotheses: First, in *MYCN*-amplified NB co-amplification of the *MYCN* gene locus and of distal regulatory regions is frequently observed within a roughly 1Mb amplicon(13, 16). Second, when amplified, hyper-abundant MYCN protein saturates high-affinity binding sites at promoters of house-keeping genes and in turn invades lower affinity sites at the promoters and enhancers of tissue-specific genes(13).

To test these two hypotheses, we performed ChIP-Seq for CDK9 and integrated its genome-wide occupancy with our MYCN and chromatin landscapes(35) in *MYCN*-amplified NB. Addressing the first hypothesis, we identify strong enrichment for CDK9 at both the *MYCN* promoter and the distal super-enhancer (Figure 4A). Investigating the second hypothesis of MYCN global effects, we observe widespread binding of MYCN to both promoters and enhancers co-incident with binding of CDK9 (Figure 4B). We and others have shown that the effect of Myc protein transcriptional regulation at target genes is proportional to the amount of Myc present at the promoter and nearby enhancers(13, 36). At individual loci in Kelly cells, we observed a concentration-dependent relationship between overall MYCN occupancy, and the magnitude of expression downregulation caused by CYC065 treatment at 1hr. *GATA2*, a developmental TF associated with the adrenergic state of MYCN-driven NB(10, 12), possesses abundant MYCN and CDK9 binding at upstream enhancers. Its gene expression was potently down-regulated by CYC065 without substantial perturbation of CDK9 occupancy (Figure 4C). In contrast, *SRSF6* and *BRD3*, genes with decreasing MYCN and CDK9 promoter/enhancer occupancy respectively, exhibited more modest sensitivity to CYC065 (Figure 4D-E). Overall, CYC065 treatment leads to global downregulation of gene expression as significantly downregulated genes outnumber upregulated genes by ~10:1 (Figure 4F). Ranking the top 5,000 genes by MYCN occupancy, we find that CYC065's effect on gene expression is concordant with

MYCN occupancy (Figure 4G). Consistent with our two hypotheses, these data suggest that CDK9 occupies *MYCN's* own super-enhancer and that CYC065 treatment selectively down-regulates genes with elevated MYCN binding at their promoters and enhancers.

Previously, NB tumors have been shown to adopt and interconvert between two lineage-derived and transcriptionally encoded states (adrenergic or mesenchymal core-regulatory circuits, CRC), expression of which is maintained by interactions between groups of TFs and enhancers and super-enhancers(11, 33, 34). Interestingly TFs that comprise the adrenergic CRC show strong interactions with MYCN. MYCN binds the enhancers of these TFs, co-binds with these TFs at other enhancers across the genome, and knockdown of these adrenergic CRC TFs downregulates MYCN regulation of tissue specific gene expression(10-12). With CYC065, we observed a selective depletion of CRC TFs driving the adrenergic state of NB, as compared with the perturbation of mesenchymal master regulator TFs (Figure 4H). Overall these data are consistent with the ability of CYC065 to selectively deplete MYCN and thus preferentially downregulate these highly MYCN-occupied genes which cross-correlate with the MYCN-associated adrenergic gene expression program that is essential for NB growth.

CYC065 targets the adrenergic state

Observing that CYC065-mediated downregulation of MYCN selectively targets TFs defining adrenergic NB state, we next sought to see if the converse was true — would MYCN overexpression convert mesenchymal NB into a more adrenergic state? Here, we utilized the SH-EP NB cell line which has demonstrated mesenchymal identity(12) and no evidence of *MYCN* genomic amplification or expression. Using retroviral transgene expression systems, we created stable SH-EP cells overexpressing wild type MYCN as well as the phosphorylation-deficient mutants (T58A, S62A, and the combined T58A S62A double mutant) all under the control of an exogenous promoter (Figure 5A). Phosphorylation of Myc proteins at both the highly conserved T58 and S62 residues is required for their proteasome-dependent turnover and these mutants (especially the T58A) are considered to be more stable and oncogenic(37). In contrast to endogenously *MYCN*-amplified NB, treatment with CYC065 failed to decrease exogenous MYCN levels in these cells (Figure 5A). Across MYCN phosphorylation-deficient mutant variants, MYCN binding at promoters and enhancers was unchanged upon CYC065 treatment (Supplemental Figure 7A,B), with the exception of the

T58A S62A double mutant, which exhibited a global decrease in MYCN occupancy (Supplemental Figure 7C,D). These data are consistent with our prior conclusions that CYC065 selectively targets nascent *MYCN* transcription specifically in the context of endogenous *MYCN* amplification.

Overexpression of MYCN in SH-EP cells increases cellular growth rate, but also renders these cells more sensitive to growth inhibition induced by CYC065 treatment (Figure 5B; Supplemental Figure 2D,7E). This result is surprising given that MYCN levels were not depleted in the context of exogenous MYCN expression. The effect was more obvious in the hyperstabilized, MYCN phosphorylation-deficient mutants. For mutants containing T58A, sensitivity to CYC065 treatment correlated with increased PARP cleavage (Figure 5B-D). These observations led us to hypothesize that MYCN overexpression altered the underlying cell state of SH-EP cells, potentially inducing a mesenchymal to adrenergic cell state transition. Using RNA-Seq, we profiled the transcriptomes of the various MYCN-overexpressing SH-EP cells and compared them to parental SH-EP cell gene expression profiles. Across all MYCN overexpression variants, we observed downregulation of genes encoding for mesenchymal identity as defined from more general molecular signature databases (Figure 5E) and specifically defined in mesenchymal NB subtypes (Figure 5F). Loss of mesenchymal gene expression coincided with an increase in expression of adrenergic-specific NB genes (Figure 5F). Using cell count-normalized gene expression, we again observed that CYC065 treatment globally downregulates gene expression with >95% of active genes downregulated. Only a small number of lowly expressed genes (< 5 FPKM) are appreciably upregulated (left edge Figure 5G). Amongst downregulated genes, mesenchymal gene signatures were the least downregulated (Figure 5G), suggesting that mesenchymal-encoding genes are not strongly occupied by MYCN. This finding is reinforced in Figure 5H-I showing that adrenergic signatures are more strongly downregulated than mesenchymal signatures by CYC065. These data suggest that MYCN overexpression converts NB to an adrenergic state and that CYC065 is able to target this state independent of any direct action against MYCN, by selectively downregulating MYCN-induced adrenergic gene expression.

CYC065 selectively inhibits growth of *MYCN*-amplified NB in vivo

As CYC065 is currently in early phase clinical evaluation in adults, we investigated its efficacy in murine models of NB. CYC065 induced significant tumor growth inhibition and increased overall survival in mice

carrying *MYCN*-amplified Kelly NB tumor xenografts but had weaker effects against non-MYCN expressing SK-N-AS NB tumor xenografts (Figure 6A-B), consistent with the modest effect on c-Myc level (Supplemental Figure 8F). CYC065 has no effect on tumor xenografts from H128 cells (Supplemental Figure 8A), which is a non-Myc driven small cell lung cancer(9). In the extensively studied TH-*MYCN* murine model of NB where MYCN is expressed under control of the tyrosine hydroxylase promoter, we administered CYC065 either orally or by intraperitoneal injection (Figure 6C, Supplemental Figure 8B-C). Here, single-agent CYC065 treatment resulted in robust inhibition of tumor growth, and together with the DNA-damaging agent temozolomide, which is commonly used in the setting of treatment-refractory NB, we observed tumor eradication and remarkable extension of overall survival. Finally, we tested CYC065 in an established transgenic model of NB, in which co-expression of hyperactivated anaplastic lymphoma kinase (ALK^{F1174L}, a clinical mutation that co-segregates with *MYCN* amplification in NB patients) drives transcriptional activation of MYCN and formation of aggressive NB(38). In the TH-ALK^{F1174L}/TH-*MYCN* genetically engineered mouse model (which expresses very high levels of murine MYCN as a consequence of direct activity of ALK on the endogenous *Mycn* promoter)(38), we observed tumor regression and a dramatic increase in overall survival compared to vehicle control (Figure 6D). These effects occurred at well-tolerated doses of CYC065 (Supplemental Figure 8D) suggesting a clear therapeutic index for CYC065 in the most highly aggressive MYCN-deregulated forms of NB.

We next determined whether CYC065 inhibition depleted endogenous MYCN, decreased transcriptional elongation, and induced apoptosis in our animal models. In *MYCN*-amplified Kelly NB tumor xenografts, we observed rapid loss of MYCN protein, induction of apoptosis and decreased RNAPII Ser2P (Figure 6F, Supplemental Figure 8E). In TH-ALK^{F1174L}/*TH-MYCN* tumors, we observed selective loss of the endogenous murine *Mycn* allele and a less pronounced effect on the exogenous human *MYCN* allele (Figure 6E). These data are consistent with our prior results(13) establishing CDK9 as a critical regulator of endogenous *MYCN* transcription. As with the previous in vitro studies, we observed increases in caspase 3 and PARP cleavage concomitant with MYCN loss in both Kelly NB tumor xenograft and TH-*MYCN* tumors following treatment with CYC065 (Figure 6F-H). Pharmacodynamic effects of CYC065 treatment were also characterized by a change in the non-invasive functional magnetic resonance imaging (MRI) spin lattice relaxation time (T_1) and apparent diffusion coefficient (ADC), which reflect a change in tissue integrity(39) and were indicative

of further rapid reduction in tumor burden (Figure 6I,J; Supplemental Figure 8G-I). Taken together, the data establish that the in vivo activity of CYC065 against MYCN-dependent NB tumor progression proceeds largely through transcriptional depletion of MYCN, leading to increased apoptosis and rapid loss of tumor burden. In other cancers with Myc deregulated and non-deregulated subtypes, we observe similar trends with selective inhibition of Myc-deregulated tumors coinciding with loss of Myc (Supplemental Figure 8J).

Discussion

In this study, we establish that *MYCN*-amplified or *MYCN*-deregulated NB can be selectively targeted via combined CDK9/2 inhibition using CYC065, an orally bioavailable and clinically well-tolerated compound for which testing in paediatric patient population is now warranted. In the preclinical setting, several multi-CDK inhibitors that also inhibit both CDK2 and CDK9 have been shown to have varying ability to downregulate MYCN and kill NB cells(17, 40). Our data build upon previous preclinical(17, 40) and clinical studies of CDK inhibition in NB including: 1) dinaciclib, a broad spectrum, but poorly-tolerated clinical inhibitor of CDKs (including CDK 1,2,5,9), which exhibited antiproliferative activity as a single agent and together with chemotherapy in NB cell-lines and in vivo models; and 2) seliciclib (CYC202, *R*-roscovitine), an inhibitor of CDK2/5/7/9 that exhibited only partial activity against MYCN and was further limited by lack of potency and rapid clearance(22, 23). Here, we show that the developmental clinical drug CYC065 — a potent and selective CDK9/2 inhibitor with enhanced pharmacokinetic and pharmacodynamics properties — is highly effective against NB. Furthermore, we demonstrate mechanistically that CYC065 effects against high-risk MYCN-driven NB are a result of CDK9 inhibition resulting in selective loss of MYCN nascent transcription, which in turn leads to cell growth arrest, and in addition sensitizes NB cells to apoptosis upon concomitant inhibition of CDK2 by the drug.

Recent work to characterize chromatin and transcriptional states in NB has more clearly defined how amplified *MYCN* invades enhancers and super-enhancers of tissue specific TFs to reshape gene expression and thereby enforce expression of a lineage-associated adrenergic state(10, 12). This invasion occurs only at oncogenic levels of MYCN and results in a highly interconnected and auto-regulatory transcriptional circuitry in which MYCN regulates multiple adrenergic identity TFs (such as *GATA2*) that in turn also regulate both *MYCN* itself and tissue-specific enhancers invaded by MYCN(10, 11). Our data support a model in

which CYC065 selectivity arises in part from the ability of CDK9 inhibition to collapse this transcriptional regulatory circuitry and break the autoregulatory feedback loop maintaining *MYCN* expression and adrenergic gene expression. Our results provide a mechanistic basis for the observed 'transcriptional addiction' of these NB cells and further reinforce the emerging idea that drugs targeting core components of the transcriptional machinery can have a therapeutic index, especially in Myc-deregulated tumors(41). In addition to canonical enhancer or E-box driven MYCN transcription, increased expression of MYCN could also be mediated by induction of *MYCNOS* (also known as *NYCM*), a regulatory antisense RNA, or other well-characterised lncRNA located within the MYCN amplicon. *MYCNOS* transcript modulates the *MYCN* locus by recruiting chromatin modifiers and TFs, resulting in enhanced *MYCN* expression, and therefore logically could be inhibited by CYC065 treatment(42). Detailed study of these mechanisms is a future priority. Oncogenic dysregulation of Myc has also been directly associated with increased translational activity either through direct upregulation of rRNA and tRNA transcription(43-45), increased expression of core ribosomal proteins(46), or with perturbation of more selective mechanisms such as targeting of eIF4A mediated translational initiation(47). Additionally, rate-limiting control of translation taking place under conditions of normal tissue homeostasis is derepressed by oncogenic levels of Myc.

Additionally, the ability of NB tumors to interconvert between adrenergic and mesenchymal identity also implicates cell state change as an anticipatable mechanism for achieving CYC065 resistance that could potentially be overcome by selective targeting of mesenchymal identity. Mesenchymal NB tumors are characterized by activated NOTCH signalling, and NOTCH-inhibiting gamma secretase inhibitors have demonstrated some efficacy against NB models(48, 49). Whether combined targeting of adrenergic and mesenchymal identity is sufficient to establish antagonistic pleiotropy and further collapse NB tumors remains to be seen. Moreover, these data suggest that transcriptional inhibitors like CYC065 will be more effective when used in combination rather than as a single agent — a conclusion supported by multiple observations of epigenetic and cell-state mediated resistance to the BET-bromodomain family of transcriptional inhibitors(50). In NB, the strong combined effect we observed with CYC065 in combination with temozolomide, which is used for therapy resistant NB, supports the addition of CYC065 as a means to selectively target MYCN-driven adrenergic identity.

Overall, we demonstrate that dual inhibition of CDK9 and CDK2 attacks MYCN dependence in NB through several mechanisms including: 1) selective blockade of CDK9 and super-enhancer-regulated nascent endogenous *MYCN* transcription; 2) induction of CDK9/2-mediated pro-apoptotic pathways; and 3) selective targeting of MYCN-regulated adrenergic gene expression in NB. Importantly, both CDK9 and CDK2 inhibition are required for maximal effect of CYC065 as CDK9 inhibition alone downregulates MYCN, but fails to induce robust apoptosis and CDK2 knockout alone is well-tolerated in NB cells. Promising results from Mosse and colleagues(51) and our own recent work(20) additionally suggests the ability of proapoptotic agents such as BCL2 inhibitors (eg. venetoclax) to further enhance effects of transcriptional inhibition. Together, these data establish a compelling therapeutic rationale for rapid clinical evaluation of dual CDK9/2 inhibitors, and specifically the oral developmental drug CYC065, in MYCN-driven high-risk NB.

Methods:

Cell culture. Cell lines were LGC standards and purchased from the European Collection of Authenticated Cell Cultures (ECACC), the American Type Culture Collection (ATCC) and Leibniz Institute DSMZ-German Collection of Microorganisms and Cell Cultures, and were cultured in RPMI-1640 (Sigma-Aldrich) or DMEM (Sigma-Aldrich) as recommended by the suppliers, supplemented with 10% fetal calf serum (FCS) (Gibco), and were maintained at 37°C under 5% CO_2 in air. All cell lines were verified by STR profiling and routinely tested for mycoplasma contamination.

Reagents. CYC202 (seliciclib, *R*-Roscovitine), CCT68127 and CYC065 were kindly provided by Cyclacel Ltd, Dundee, Scotland, UK. Cycloheximide (C4859) and Actinomycin D (A9415) were purchased from Sigma-Aldrich and MG132 (1748) from Tocris Bioscience. Temozolomide, Flavopiridol, Palbociclib, Dinaciclib and SNS-032 was purchased from SelleckChem. BAY 1145372 was purchased from Activebiochem. Compound 3 was kindly provided by Keith Jones, ICR, London, UK. THZ1 (A8882) was purchased from Stratech. NVP-2 was obtained from by Calla Olson, Baylor College of Medicine, Houston, Texas, USA. THAL-SNS-032 was synthesized in the Gray lab.

Tumor Cell Proliferation Assays. Cell proliferation assays were performed as described(52) using the Sulforhodamine B (230162; SRB) assay or using CellTiter-Glo Luminescent Cell Viability Assay (G7571; Promega) and read on a Synergy HT Multi-Mode Microplate Reader (Biotek). GI50 values were calculated in PRISM GraphPad and the GI50 was defined as the compound concentration at which tumor cell growth was inhibited by 50% compared with the vehicle control. Percentage of viable cells was analysed using trypan blue exclusion method.

CDK2 activity detection. The lentivirus construct of CDK2 sensor is kindly provided by Dr. Sabrina L. Spencer, Boulder, U.S.A. The CDK2 sensor lentiviral particles were produced using second-generation packaging plasmids psPAX2 and pMD2.G obtained from Addgene (a gift from Thomas F. Westbrook, Baylor College of Medicine, Addgene plasmids 1226 and 12259). 293T cells were cultured in DMEM (Sigma-Aldrich) supplemented with 10% FCS and transfected using TransIT®-293 Transfection Reagent (MIR 2704; Mirus). Viral supernatant was collected 48 and 72hr after infection, filtered through a 0.45-μm low protein

binding filter (HAWP04700; EMD Millipore), and concentrated with a Lenti-X concentrator (631232; Clontech). Kelly and BE(2)C cells were transduced with concentrated virus in the presence of 8µg/ml polybrene. After 24hr, cells were fed with DMEM with 10% FCS. mVenus positive cells were collected using flow cytometry after 72hr infection. mVenus positive cells were plated in glass bottom 96-well microplate (655892; Greiner Bio-One). After 24hr, cells were treated with DMSO, 1xGI50 NVP-2, 2xGI50 NVP-2 or 1xGI50 CYC065 for 2hr, 4hr, 6hr or 8hr. Cells were fixed by 4% paraformaldehyde and followed by DAPI staining. mVenus fluorescence was imaged by IC200 cytometer (ValaSciences).

Immunofluorescence. Immunofluorescence analysis was performed as described(52). Briefly, cells were fixed with ice-cold 4% paraformaldehyde, permeabilized with 0.2% Triton X-100 in PBS, incubated with primary antibody, Alexa Fluor® 488 or Alexa Fluor® 568 secondary antibody (Life Technologies) and visualized with a Leica DM2500 microscope or quantified with the InCell Analyzer 1000.

Click-iT RNA imaging Kit. The Click-iT RNA imaging assay (C10330, ThermoFisher) was used to detect newly synthesized RNA, by incorporating an alkyne-containing nucleoside into the newly synthesized RNA, which was detected by an azide containing a fluorescent dye. The assay was conducted according to manufacturer protocol. Briefly, cells were co-treated with 1mM 5-ethynyl uridine and either DMSO, 1µM CYC065 or 1µM CCT68127 for 60 minutes. As a positive control, the general transcription inhibitor Actinomycin D (0.5µg/ml, 60 minutes incubation) was used. The cells were fixed and permeabilized as described above, incubated with Click-iT reaction cocktail and nuclei stained with DAPI. Fluorescence was visualized with a Leica DM2500 microscope and quantified with the InCell Analyzer 1000. Green fluorescence indicated newly synthesized RNA. Nascent RNA was isolated using the Click-iT Nascent RNA Capture Kit (C10365, ThermoFisher), followed by qPCR. Primers for PCR is listed in Table 1.

Fluorescence *in situ* hybridisation (FISH). MYCN FISH (05J50-001, Abbott Molecular) was conducted according to the manufacturer‘s protocol. Briefly, Kelly cells were treated with CYC065, fixed with Carnoy’s solution and co-denatured with LSI N-MYC (2q24) Spectrum Orange probe. The melting temperature set at 73°C (2 minutes) and hybridisation temperature at 37°C (overnight). The cells were visualized using a Leica DM2500 microscope. Non *MYCN*-amplified cells, SK-N-AS and SH-EP, were used as controls.

Western Blot. Western blot analysis was performed as described(52) using NuPAGE Novex 4-12% and the membranes were exposed using a Fujifilm LAS-4000 Imager, with the Amersham ECL Prime Western Blotting Detection Reagent (GE Healthcare). Antibodies for immunoblots is listed in Table 2.

shRNA knockdown. shRNA knockdown experiment was performed SKNBE cells, protein was harvested 96hr after virus transduction and subjected to Western blot analysis. shRNA for CDK7 and CDK9 (shRNA TRC library) were purchased from Sigma-Aldrich and listed in Table 3. SHC002 MISSION pLKO.1-puro Non-Mammalian shRNA Control was used as negative control.

siRNA knockdown. siRNA knockdown experiment was performed Kelly cells, protein was harvested 96hr after transfection with siRNA and Dharmafect (Dharmacon) and subjected to Western blot analysis. siRNA for CDK2 (J003236-12/14) and CDK9 (J003243-14) were purchased from Dharmacon. Non-targeting siRNA control was used as negative control.

Generation of CDK2 CRISPR cell lines. To generate Cas9 stable cell lines, Kelly cells transduced with 1ml virus and and 8 µg/ml Polybrene (Merck Millipore) for 48hr, selected with 10µg/ml blasticidin for 10 days, sorted into single cells and check for expression of Cas9. Virus were created by transfection of 293T cells with Viral Power mix (Invitrogen) and a pLenti-Cas9-2A-Blast plasmid(53) (a gift from Jason Moffat, University of Toronto, Addgene #73310).

To generate CDK2 CRISPR stable cell lines, Cas9 stable Kelly cells were transduced with 1ml virus and and 8µg/ml Polybrene (Merck Millipore) for 48hr, selected with 1µg/ml puromycin for 10 days, sorted into single cells and check for loss of expression of CDK2. Virus were created by transfection of 293T cells with Viral Power mix (Invitrogen) and CDK2 sgRNA (Invitrogen LentiArray Human CRISPR Library CRISPR id 692363). To validate CDK2 knockout, genomic DNA was extracted (Zymo Quick-DNA microprep, Zymo Research D3020) and sequences of the locus around the putative edit were PCR-amplified using target-specific primers (CDK2 sgRNA (CRIPSR ID 692363) forward: 5´-CACCCTGACTACCCAAGAATTAG-3´, reverse: 5´-TGTCAGCCCAGAGAGGATAA-3). The resulting PCR products were purified (DNA clean and

concentrator-25, Zymo Research D4033) and submitted to Sanger sequencing and analyzed using online ICE CRISPR Analysis Tool (https://www.synthego.com/products/bioinformatics/crispr-analysis).

Flow cytometry. Cells were treated with CYC065 or CCT68127, fixed in cold 70% ethanol, treated with 40ug/ml propidium iodide (P4864; Sigma Aldrich) and 100ug/ml RNase A (19101; Qiagen) before analysed using LSR II flow cytometer (BD Bioscience).

Promoter Activity Luciferase Reporter Assay. IMR-32 cells were transfected with a MYCN promoter Renilla luciferase construct and Cypridina TK control construct (SN0322s; Switchgear Genomics), re-plated to 96-well plates and treated with compounds (1 µM) for 6hr at 48hr post transfection. Luciferase reading was normalized to the Cypridina TK control signal.

Tandem ubiquitin binding entity (TUBE) pulldown. Kelly cells were treated with either DMSO or 1uM CYC065 for the indicated time, lysed in 50mM Tris-HCl pH 7.5, 150mM NaCl, 1mM EDTA, 1% NP-40, 10% glycerol and 200ug/ml GST-TUBE2 (UM102; Biosensors, 2BScientific) or in the absence of GST-TUBE2 for control pulldown. Pierce Glutathione Magnetic Beads (88821; Thermo Scientific Fisher) were used to pulldown ubiquitinated proteins from cell lysates according to manufacturer instructions. Ubiquitinated proteins were eluted by boiling beads in Laemmli buffer and resolved by SDS-PAGE.

Quantitative RT-PCR and ChIP. Quantitative RT-PCR and ChIP analysis was performed as described(52). Fluorescence was read using Step One Plus Real-Time PCR system (Applied Biosystems) using the TaqMan CT/CT program. Analysis was performed using the Step One software. Taqman assays for qPCR is listed in Table 1. The error bars show SD of representative replicate. Primers specific for APEX gene were forward: TGAAGCGGGTGTTAGTATGATCT and reverse: ACCACAAACAACAGAACGAATCT.

p53 mutational analysis. Genomic DNA was extracted from cell lines (Qiagen QIAamp DNA kit). PCR amplification of exons 5 – 9 was performed using the primers shown in Table 4. Products were sequenced with the original PCR primers using the BigDye Terminator Cycle Sequencing Kit and an ABI 3730 Genetic

Analyzer (Applied Biosystems). Sequences were analysed using Mutation Surveyor software v3.97 (SoftGenetics).

RNA sequencing. RNA extraction was performed by Direct-zol RNA miniprep kit (R2050; Zymo Research) with recommended DNase I digestion according to the manufacturer's instructions. All samples were subjected to quality control on a Tapestation instrument and only RNA with RIN (RNA Integrity Number) > 8 were used for sequencing. External RNA spike-ins (ERCC, Ambion) were added to total RNA based on cell number. Total RNA and ERCC were subjected to poly(A) selection (E7490; New England BioLabs Inc.). Library preparation of RNA sequencing is performed by using NEBNext® Ultra™ Directional RNA Library Prep Kit for Illumina® (E4720L; New England BioLabs Inc.). RNA sequencing libraries were sequenced on a NextSeq 500 (Illumina, San Diego, Calif). GEO session information of RNA-Seq experiments is in Table 7.

Chromatin immunoprecipitation using tagmentation (ChIPmentation). Antibodies for ChIPmentation were purchased as follows: MYCN (sc-791; Santa Cruz Biotechnology), H3K27ac (8173S; Cell signaling Technology). ChIPmentation was performed as previously described(54). ChIPmentation libraries were sequenced on a NextSeq 500 (Illumina, San Diego, Calif).

ATAC-Seq analysis. For each cell line, 50,000 cells were lysed for 10 minutes at 4 °C in lysis buffer (10mM Tris-HCl pH 7.4, 10mM NaCl, 3mM MgCl2, and 0.1% IGEPAL CA-360). After lysis, the pellets were subjected to a transposition reaction (37 °C, 60 minutes) using 2× TD buffer and transposase enzyme (Illumina Nextera DNA preparation kit, FC-121-1030). The transposition mixture was purified using a Qiagen MinElute PCR purification kit. Library amplification was performed using custom Nextera primers, and the number of total cycles was determined by running a SYBR-dye-based qPCR reaction and calculating the cycle number that corresponded to one-fourth the maximum. Amplified libraries were purified using a Qiagen PCR purification kit and sequenced on a single lane of an Illumina NextSeq.

ChIP-Seq analysis. MYCN and H3K27ac ChIP-Seq data in the Kelly cell line were obtained from Zeid et. al., *Nature Genetics*, 2018. Briefly, raw reads were aligned using Bowtie2 (version 2.2.1) to build version

NCBI37/HG19(55). Alignments were performed using all default parameters except for –N 1. These criteria preserved only reads that mapped uniquely to the genome with one or fewer mismatches. All analyses were performed using HG19 RefSeq gene annotations.

Normalized read density of a ChIP-Seq dataset in any genomic region was calculated using the Bamliquidator read density calculator (https://github.com/BradnerLab/pipeline/wiki/bamliquidator). ChIP-Seq reads aligning to the region were extended by 200bp and the density of reads per base pair (bp) was calculated. The density of reads in each region was normalized to the total number of million mapped reads producing read density in units of reads per million mapped reads per bp (rpm/bp).

Regions of H3K27ac and MYCN enrichment were defined using MACS version 1.4.1 (Model based analysis of ChIP-Seq) peak finding algorithm at a p-value threshold of 1e-9(56). Active promoters were defined as those with an enriched H3K27ac peak in the +/-1kb region flanking the transcription start site (TSS). Active enhancers were defined as regions of H3K27ac outside of this +/-1kb TSS region. For each gene, MYCN promoter and enhancer load was quantified as the cumulative area under curve MYCN signal in the +/-1kb region (promoter) or within +/-50kb of the TSS (enhancer).

To correlate expression change with MYCN load in Kelly, we first defined active transcribed and expressed genes as those with H3K27ac present in the +/-1kb TSS region and expression in the top 50% of all genes. We ranked these genes by promoter + enhancer MYCN load and binned the top 5,000 genes into 5 bins of 1,000 genes each. For each bin, average MYCN load was calculated as was the average $\log_2$ change in mRNA levels after 1hr CYC065 treatment (Figure 4G). Error bars represent the 95% confidence intervals of the mean as empirically determined by resampling of the data with replacement (10,000 iterations). Sequencing depth of ChIP-Seq experiments is in Table 5.

ChIPmentation analysis. MYCN and H3K27ac ChIPmentation data in SH-EP MYCN cells were analyzed using AQUAS TF and histone ChIP-Seq pipeline (https://github.com/kundajelab/chipseq_pipeline). All analyses were performed using HG19 RefSeq gene annotations. Normalized read density of a ChIPmentation dataset in any genomic region was calculated as described in ChIP-Seq analysis. Regions

of H3K27ac and MYCN enrichment were defined using MACS2 peak finding algorithm built in AQUAS TF and histone ChIP-Seq pipeline at a p-value threshold of 1e-5. Active promoters and active enhancers were defined as described in ChIP-Seq analysis.

Gene expression analysis. Total RNA was isolated from cells and tumor tissue using the RNAeasy plus minikit (Qiagen), labelled and hybridized to Gene Chip® human or mouse transcriptome expression array (Affymetrix). Samples were RMA normalized using the “limma” package from R and differentially expressed genes were called using a linear model and empirical Bayes statistics from the “affy” package. For heat maps showing gene expression changes, genes were filtered based on average expression (log_2 intensity value >5) and hierarchical clustering using Manhattan distance with complete linkage was done in R. Gene set enrichment analyses (GSEA)(57) were performed with the C2 and Hallmark gene set collections from MSigDB, signal2noise metric and 1000 permutations. mRNA half-lives were taken from Schwannhäuser et al., grouped in short (<5h) and long (>18h) half-life and the log_2 fold change in mRNA expression upon CYC065 treatment was illustrated as box plot. Boxes represent the first and third quartile, the middle line reflects the median and whiskers extend to 1.5x interquartile range. Outliers are shown as dots. p-values were calculated with a two-tailed Wilcoxon rank sum test. The log_2 fold change of median of ADRN CRC or MES CRC upon DMSO group was represent using heatmap.

RNA sequencing analysis of SH-EP MYCN cell lines. Reads were aligned to the human reference genome hg19/GRCh37 using HISAT2 with parameter --no-unal. Gene expression values (FPKM=fragments per kilobase per million reads) were computed by Cufflinks v2.2.1 using library type fr-firststrand. Cell number normalized FPKM were calculated based on ERCC RNA spikein. ADRN and MES gene sets were taken from Van *et. al.* 2017 *Nat. Genet* and the log_2 fold change in mRNA expression upon SH-EP or DMSO group was illustrated as box plot. Boxes represent the first and third quartile, the middle line reflects the median and whiskers extend to 1.5x interquartile range. The P-values were calculated with a two-tailed Welch’s t-test. Gene set enrichment analyses (GSEA)(57) were performed with the C2 and Hallmark gene set collections from MSigDB, Signal2Noise metric and 1000 permutations. The log_2 fold change of median of ADRN CRC or MES CRC upon DMSO group was represent using heatmap.

Study Approval. All experimental protocols were monitored and approved by ICR Animal Welfare and Ethical Review Body, in compliance with guidelines specified by the U.K. Home Office Animals (Scientific Procedures) Act 1986 and the United Kingdom National Cancer Research Institute Guidelines for the Welfare of Animals in Cancer Research(58).

In vivo efficacy of CYC065 in human NB xenograft models and TH-*MYCN* and GEM mice. Female CrTac:NCr-*Foxn1*^{nu} athymic nude mice (Taconic, USA) (6 weeks of age) were injected with either Kelly (5.10^6 cells), SK-N-AS (5.10^6 cells) or H128 (5.10^6 cells) subcutaneously in one flank and allowed to establish. Mice bearing NB xenografts with a mean diameter of 5mm were treated with 75mg/kg/day CYC065 or vehicle (saline) p.o., with a 'five days on, two days off' schedule for up to 3 weeks. Tumor volumes were measured by Vernier caliper across two perpendicular diameters, and volumes were calculated according to the formula: $V = 4/3\pi\ [(d1 + d2) / 4]^3$. Transgenic TH-*MYCN* or TH-*ALK*^{F1174L}/*TH-MYCN* mice were genotyped to detect the presence of human MYCN or ALK transgene (59). Male or female mice with palpable tumors (30–50 days old) treated with 50mg/kg of CYC065, CCT68127, vehicle (saline), freshly prepared 6mg/kg temozolomide or with a combination of either 50mg/kg of CYC065 or 50mg/kg of CCT68127 with freshly prepared 6mg/kg temozolomide for two consecutive weeks. CYC065 or CCT68127 were dosed in a 'five days on, two days off' schedule. Mice were allowed access to sterile food and water *ad libitum*.

MRI. Changes in tumor volume in the TH-*MYCN* or TH-*ALK*^{F1174L}/*TH-MYCN* mice were quantified using MRI on a 7T horizontal bore MicroImaging system (Bruker Instruments) using a 3 cm birdcage coil. Anatomical T_2-weighted coronal images were acquired through the mouse abdomen, from which tumor volumes were determined using segmentation from regions of interest (ROI) drawn on each tumor-containing slice. The spin-lattice relaxation time (T_1) and the apparent diffusion coefficient (ADC), two functional MRI parameters, were also measured(39). At trial end, tumors were dissected and fixed with 4% paraformaldehyde or snap frozen in liquid nitrogen for further analysis.

Pathology. Tissue sections were stained with haematoxylin and eosin or specific antibodies. Immunohistochemistry was performed using standard methods. Briefly, 5µm sections were stained with

antibodies, including heat-induced epitope retrieval of specimens using citrate buffer (pH 6) or EDTA buffer, and scored by a consultant histopathologist.

Tumor or spleen tissue was homogenized using T-PER buffer (Thermo Scientific Fisher) containing proteinase inhibitor (Roche) and a cocktail of phosphatase inhibitors (Santa Cruz). Protein (30 mg) was denatured in lithium dodecyl sulfate sample buffer (Invitrogen), separated on precast 4%–12% Bis-Tris gels (Invitrogen), and transferred to nitrocellulose membranes for western blotting. Immunoblots were recorded electronically on a Fujifilm LAS-4000 scanner.

Statistical analysis. Data were visualized, and statistical analyses performed using GraphPad Prism (version 6; GraphPad Software Inc.) or R statistical package. For each group of data, estimate variation was taken into account and is indicated in each figure as S.D. or S.E.M. If single data are presented, these data are representative of biological or technical triplicates, as indicated. Statistical analyses between groups with comparable variance was performed using a two-tailed unpaired Student's *t*-test unless otherwise indicated. Pearson's tests were used to identify correlations among variables. Significance for all statistical tests was shown in figures or legends. $P<0.05$ is considered significant. No samples or animals were excluded from analysis, and group sizes was determined by power analyses using data previously shown(39, 52). Animals were randomly assigned to groups. Studies were not conducted blinded, with the exception of all histopathological scoring.

Data Availability. ChIP-seq and RNA-seq data is available in GEO series GSE107126, GSE80151, GSE128330, GSE145068.

Author Contributions:

Conception and design: E.P., T.L., Y.J., C.Y.L., and L.C.

Conduct of the experiments, data analysis, and interpretation: E.P., T.L., Y.J., R.Z., S.W., C.K., A.H., K.B., Z.U., K.T., R.Z., A.H., G. B., M.E.E., M.P.L., Y.S., G. L., E.C., B.M.C, M.V., A.D.H.B., H.W., N.T., G.S.A, R.C., G.B., M.W.R., G.B., A. F., R. B., P.A.C., J.D.B., N.S.G., J.B., S.P.R., S.A.E., D.Z., P.W., J.E.B., J.M., I.V., M.E., C.Y.L. and L.C.

Manuscript writing: E.P., T.L., Y.J., P.W., M.E., C.Y.L. and L.C.

All authors read and approved the final manuscript.

Acknowledgements:

We acknowledge the support received from CRUK (programme/project funding), Children with Cancer UK (project), Christopher's Smile, INSTINCT, SPARKS, The Neuroblastoma Society and EU Marie Curie. We also acknowledge the support received from ICR, CRUK and EPSRC Cancer Imaging Centre (C1060/A10334), and to ICR CRUK Imaging Centre (C1090/A16464), in association with the MRC and Department of Health (England), CRUK funding to our CRUK ICR Centre and The Wellcome Trust (grant 091763Z/10/Z). C.Y.L is a Pew Stewart Scholar for Cancer Research, a CPRIT Scholar in Cancer Research (RR150093), and is supported by the NIH and NCI (1R01CA215452-01). Y.J. is a Children with Cancer UK Research Fellow. S.W. and M.E. were supported by the German Federal Ministry of Education and Research - BMBF as part of the SYSMED-NB consortium. P.W. acknowledges programme grant support from CRUK (CRUK grant number C309/A11566) and support from ICR, London and Cyclacel Ltd. He is also a CRUK Life Fellow. M.W.R and R.B. acknowledge CRUK programme grant (C24461/A23302). We thank Florence Raynaud and Ruth Ruddle for PK studies, Anna Burford, Louise Howell, Ian Titley and Lisa Pickard for technical assistance, Keith Jones, Pawan Poudel and Anguraj Sadanandam for advice, and members of the Chesler laboratory for comments on the manuscript.

References

1. Dang CV, Reddy EP, Shokat KM, and Soucek L. Drugging the 'undruggable' cancer targets. *Nature reviews Cancer.* 2017;17(8):502-8.
2. Meyer N, and Penn LZ. Reflecting on 25 years with MYC. *Nature reviews Cancer.* 2008;8(12):976-90.
3. Soucek L, Whitfield J, Martins CP, Finch AJ, Murphy DJ, Sodir NM, et al. Modelling Myc inhibition as a cancer therapy. *Nature.* 2008;455(7213):679-83.
4. Dang CV. MYC on the path to cancer. *Cell.* 2012;149(1):22-35.
5. Poole CJ, and van Riggelen J. MYC-Master Regulator of the Cancer Epigenome and Transcriptome. *Genes (Basel).* 2017;8(5).
6. Rahl PB, and Young RA. MYC and transcription elongation. *Cold Spring Harbor perspectives in medicine.* 2014;4(1):a020990.
7. Baranello L, Wojtowicz D, Cui K, Devaiah BN, Chung HJ, Chan-Salis KY, et al. RNA Polymerase II Regulates Topoisomerase 1 Activity to Favor Efficient Transcription. *Cell.* 2016;165(2):357-71.
8. Nie Z, Hu G, Wei G, Cui K, Yamane A, Resch W, et al. c-Myc is a universal amplifier of expressed genes in lymphocytes and embryonic stem cells. *Cell.* 2012;151(1):68-79.
9. Lin CY, Loven J, Rahl PB, Paranal RM, Burge CB, Bradner JE, et al. Transcriptional amplification in tumor cells with elevated c-Myc. *Cell.* 2012;151(1):56-67.
10. Boeva V, Louis-Brennetot C, Peltier A, Durand S, Pierre-Eugene C, Raynal V, et al. Heterogeneity of neuroblastoma cell identity defined by transcriptional circuitries. *Nature genetics.* 2017;49(9):1408-13.
11. Durbin AD, Zimmerman MW, Dharia NV, Abraham BJ, Iniguez AB, Weichert-Leahey N, et al. Selective gene dependencies in MYCN-amplified neuroblastoma include the core transcriptional regulatory circuitry. *Nature genetics.* 2018;50(9):1240-6.
12. van Groningen T, Koster J, Valentijn LJ, Zwijnenburg DA, Akogul N, Hasselt NE, et al. Neuroblastoma is composed of two super-enhancer-associated differentiation states. *Nature genetics.* 2017;49(8):1261-6.
13. Zeid R, Lawlor MA, Poon E, Reyes JM, Fulciniti M, Lopez MA, et al. Enhancer invasion shapes MYCN-dependent transcriptional amplification in neuroblastoma. *Nature genetics.* 2018;50(4):515.
14. Puissant A, Frumm SM, Alexe G, Bassil CF, Qi J, Chanthery YH, et al. Targeting MYCN in neuroblastoma by BET bromodomain inhibition. *Cancer Discov.* 2013;3(3):308-23.
15. Dolman ME, Poon E, Ebus ME, den Hartog IJ, van Noesel CJ, Jamin Y, et al. Cyclin-Dependent Kinase Inhibitor AT7519 as a Potential Drug for MYCN-Dependent Neuroblastoma. *Clinical cancer research : an official journal of the American Association for Cancer Research.* 2015;21(22):5100-9.
16. Chipumuro E, Marco E, Christensen CL, Kwiatkowski N, Zhang T, Hatheway CM, et al. CDK7 inhibition suppresses super-enhancer-linked oncogenic transcription in MYCN-driven cancer. *Cell.* 2014;159(5):1126-39.
17. Chen Z, Wang Z, Pang JC, Yu Y, Bieerkehazhi S, Lu J, et al. Multiple CDK inhibitor dinaciclib suppresses neuroblastoma growth via inhibiting CDK2 and CDK9 activity. *Sci Rep.* 2016;6:29090.
18. Kawakami M, Mustachio LM, Rodriguez-Canales J, Mino B, Roszik J, Tong P, et al. Next-Generation CDK2/9 Inhibitors and Anaphase Catastrophe in Lung Cancer. *J Natl Cancer Inst.* 2017;109(6).
19. Frame SSCMCABSPMECPAWPBDZD. Fadraciclib (CYC065), a novel CDK inhibitor, targets key pro-survival and oncogenic pathways in cancer *PLOS ONE.* 2020.
20. Whittaker SR, Barlow C, Martin MP, Mancusi C, Wagner S, Self A, et al. Molecular profiling and combinatorial activity of CCT068127: a potent CDK2 and CDK9 inhibitor. *Mol Oncol.* 2018;12(3):287-304.

725 21. Whittaker SR, Walton MI, Garrett MD, and Workman P. The Cyclin-dependent kinase inhibitor
726 CYC202 (R-roscovitine) inhibits retinoblastoma protein phosphorylation, causes loss of Cyclin D1,
727 and activates the mitogen-activated protein kinase pathway. *Cancer Res.* 2004;64(1):262-72.
728 22. Wilson SC, Atrash B, Barlow C, Eccles S, Fischer PM, Hayes A, et al. Design, synthesis and biological
729 evaluation of 6-pyridylmethylaminopurines as CDK inhibitors. *Bioorg Med Chem.*
730 2011;19(22):6949-65.
731 23. Green S.R., Frame S., Anderson S., Hogben M., MacCallum D.E., Wood G., et al. *Proceedings of the*
732 *100th Annual Meeting of the American Association for Cancer Research*. AACR; 2009:3863.
733 24. Choudhary GS, Tat TT, Misra S, Hill BT, Smith MR, Almasan A, et al. Cyclin E/Cdk2-dependent
734 phosphorylation of Mcl-1 determines its stability and cellular sensitivity to BH3 mimetics.
735 *Oncotarget.* 2015;6(19):16912-25.
736 25. Spencer SL, Cappell SD, Tsai FC, Overton KW, Wang CL, and Meyer T. The proliferation-quiescence
737 decision is controlled by a bifurcation in CDK2 activity at mitotic exit. *Cell.* 2013;155(2):369-83.
738 26. Rye CS, Chessum NE, Lamont S, Pike KG, Faulder P, Demeritt J, et al. Discovery of 4,6-disubstituted
739 pyrimidines as potent inhibitors of the heat shock factor 1 (HSF1) stress pathway and CDK9.
740 *Medchemcomm.* 2016;7(8):1580-6.
741 27. Lucking U, Scholz A, Lienau P, Siemeister G, Kosemund D, Bohlmann R, et al. Identification of
742 Atuveciclib (BAY 1143572), the First Highly Selective, Clinical PTEFb/CDK9 Inhibitor for the
743 Treatment of Cancer. *ChemMedChem.* 2017;12(21):1776-93.
744 28. Olson CM, Jiang B, Erb MA, Liang Y, Doctor ZM, Zhang Z, et al. Pharmacological perturbation of
745 CDK9 using selective CDK9 inhibition or degradation. *Nat Chem Biol.* 2018;14(2):163-70.
746 29. Rahl PB, Lin CY, Seila AC, Flynn RA, McCuine S, Burge CB, et al. c-Myc regulates transcriptional
747 pause release. *Cell.* 2010;141(3):432-45.
748 30. He S, Liu Z, Oh DY, and Thiele CJ. MYCN and the epigenome. *Front Oncol.* 2013;3:1.
749 31. Rahl PB, and Young RA. MYC and transcription elongation. *Cold Spring Harbor perspectives in*
750 *medicine.* 2014;4(1):a020990.
751 32. Hessmann E, Schneider G, Ellenrieder V, and Siveke JT. MYC in pancreatic cancer: novel
752 mechanistic insights and their translation into therapeutic strategies. *Oncogene.*
753 2016;35(13):1609-18.
754 33. McMahon SB, Wood MA, and Cole MD. The essential cofactor TRRAP recruits the histone
755 acetyltransferase hGCN5 to c-Myc. *Mol Cell Biol.* 2000;20(2):556-62.
756 34. Gaspar-Maia A, Alajem A, Meshorer E, and Ramalho-Santos M. Open chromatin in pluripotency
757 and reprogramming. *Nat Rev Mol Cell Biol.* 2011;12(1):36-47.
758 35. Zeid R, Lawlor MA, Poon E, Reyes JM, Fulciniti M, Lopez MA, et al. Enhancer invasion shapes
759 MYCN-dependent transcriptional amplification in neuroblastoma. *Nature genetics.*
760 2018;50(4):515-23.
761 36. Lorenzin F, Benary U, Baluapuri A, Walz S, Jung LA, von Eyss B, et al. Different promoter affinities
762 account for specificity in MYC-dependent gene regulation. *Elife.* 2016;5.
763 37. Wang X, Cunningham M, Zhang X, Tokarz S, Laraway B, Troxell M, et al. Phosphorylation regulates
764 c-Myc's oncogenic activity in the mammary gland. *Cancer Res.* 2011;71(3):925-36.
765 38. Berry T, Luther W, Bhatnagar N, Jamin Y, Poon E, Sanda T, et al. The ALK(F1174L) mutation
766 potentiates the oncogenic activity of MYCN in neuroblastoma. *Cancer Cell.* 2012;22(1):117-30.
767 39. Jamin Y, Tucker ER, Poon E, Popov S, Vaughan L, Boult JK, et al. Evaluation of clinically translatable
768 MR imaging biomarkers of therapeutic response in the TH-MYCN transgenic mouse model of
769 neuroblastoma. *Radiology.* 2013;266(1):130-40.
770 40. Delehouze C, Godl K, Loaec N, Bruyere C, Desban N, Oumata N, et al. CDK/CK1 inhibitors
771 roscovitine and CR8 downregulate amplified MYCN in neuroblastoma cells. *Oncogene.*
772 2014;33(50):5675-87.
773 41. Kress TR, Sabo A, and Amati B. MYC: connecting selective transcriptional control to global RNA
774 production. *Nat Rev Cancer.* 2015;15(10):593-607.

775 42. Vadie N, Saayman S, Lenox A, Ackley A, Clemson M, Burdach J, et al. MYCNOS functions as an
776 antisense RNA regulating MYCN. *RNA Biol.* 2015;12(8):893-9.
777 43. Arabi A, Wu S, Ridderstrale K, Bierhoff H, Shiue C, Fatyol K, et al. c-Myc associates with ribosomal
778 DNA and activates RNA polymerase I transcription. *Nat Cell Biol.* 2005;7(3):303-10.
779 44. Gomez-Roman N, Grandori C, Eisenman RN, and White RJ. Direct activation of RNA polymerase III
780 transcription by c-Myc. *Nature.* 2003;421(6920):290-4.
781 45. Grandori C, Gomez-Roman N, Felton-Edkins ZA, Ngouenet C, Galloway DA, Eisenman RN, et al. c-
782 Myc binds to human ribosomal DNA and stimulates transcription of rRNA genes by RNA
783 polymerase I. *Nat Cell Biol.* 2005;7(3):311-8.
784 46. Wolf E, Lin CY, Eilers M, and Levens DL. Taming of the beast: shaping Myc-dependent
785 amplification. *Trends Cell Biol.* 2015;25(4):241-8.
786 47. Wolfe AL, Singh K, Zhong Y, Drewe P, Rajasekhar VK, Sanghvi VR, et al. RNA G-quadruplexes cause
787 eIF4A-dependent oncogene translation in cancer. *Nature.* 2014;513(7516):65-70.
788 48. van Groningen T, Akogul N, Westerhout EM, Chan A, Hasselt NE, Zwijnenburg DA, et al. A NOTCH
789 feed-forward loop drives reprogramming from adrenergic to mesenchymal state in
790 neuroblastoma. *Nat Commun.* 2019;10(1):1530.
791 49. Ferrari-Toninelli G, Bonini SA, Uberti D, Buizza L, Bettinsoli P, Poliani PL, et al. Targeting Notch
792 pathway induces growth inhibition and differentiation of neuroblastoma cells. *Neuro Oncol.*
793 2010;12(12):1231-43.
794 50. Sonawane YA, Taylor MA, Napoleon JV, Rana S, Contreras JI, and Natarajan A. Cyclin Dependent
795 Kinase 9 Inhibitors for Cancer Therapy. *J Med Chem.* 2016;59(19):8667-84.
796 51. Ham J, Costa C, Sano R, Lochmann TL, Sennott EM, Patel NU, et al. Exploitation of the Apoptosis-
797 Primed State of MYCN-Amplified Neuroblastoma to Develop a Potent and Specific Targeted
798 Therapy Combination. *Cancer Cell.* 2016;29(2):159-72.
799 52. Brockmann M, Poon E, Berry T, Carstensen A, Deubzer HE, Rycak L, et al. Small molecule inhibitors
800 of aurora-a induce proteasomal degradation of N-myc in childhood neuroblastoma. *Cancer Cell.*
801 2013;24(1):75-89.
802 53. Hart T, Chandrashekhar M, Aregger M, Steinhart Z, Brown KR, MacLeod G, et al. High-Resolution
803 CRISPR Screens Reveal Fitness Genes and Genotype-Specific Cancer Liabilities. *Cell.*
804 2015;163(6):1515-26.
805 54. Schmidl C, Rendeiro AF, Sheffield NC, and Bock C. ChIPmentation: fast, robust, low-input ChIP-seq
806 for histones and transcription factors. *Nat Methods.* 2015;12(10):963-5.
807 55. Langmead B, Trapnell C, Pop M, and Salzberg SL. Ultrafast and memory-efficient alignment of
808 short DNA sequences to the human genome. *Genome biology.* 2009;10(3).
809 56. Zhang Y, Liu T, Meyer CA, Eeckhoute J, Johnson DS, Bernstein BE, et al. Model-based analysis of
810 ChIP-Seq (MACS). *Genome biology.* 2008;9(9).
811 57. Subramanian A, Tamayo P, Mootha VK, Mukherjee S, Ebert BL, Gillette MA, et al. Gene set
812 enrichment analysis: a knowledge-based approach for interpreting genome-wide expression
813 profiles. *Proceedings of the National Academy of Sciences of the United States of America.*
814 2005;102(43):15545-50.
815 58. Workman P, Aboagye EO, Balkwill F, Balmain A, Bruder G, Chaplin DJ, et al. Guidelines for the
816 welfare and use of animals in cancer research. *British journal of cancer.* 2010;102(11):1555-77.
817 59. Weiss WA, Aldape K, Mohapatra G, Feuerstein BG, and Bishop JM. Targeted expression of MYCN
818 causes neuroblastoma in transgenic mice. *The EMBO journal.* 1997;16(11):2985-95.
819 60. Schwanhausser B, Busse D, Li N, Dittmar G, Schuchhardt J, Wolf J, et al. Global quantification of
820 mammalian gene expression control. *Nature.* 2011;473(7347):337-42.
821

Figure 1

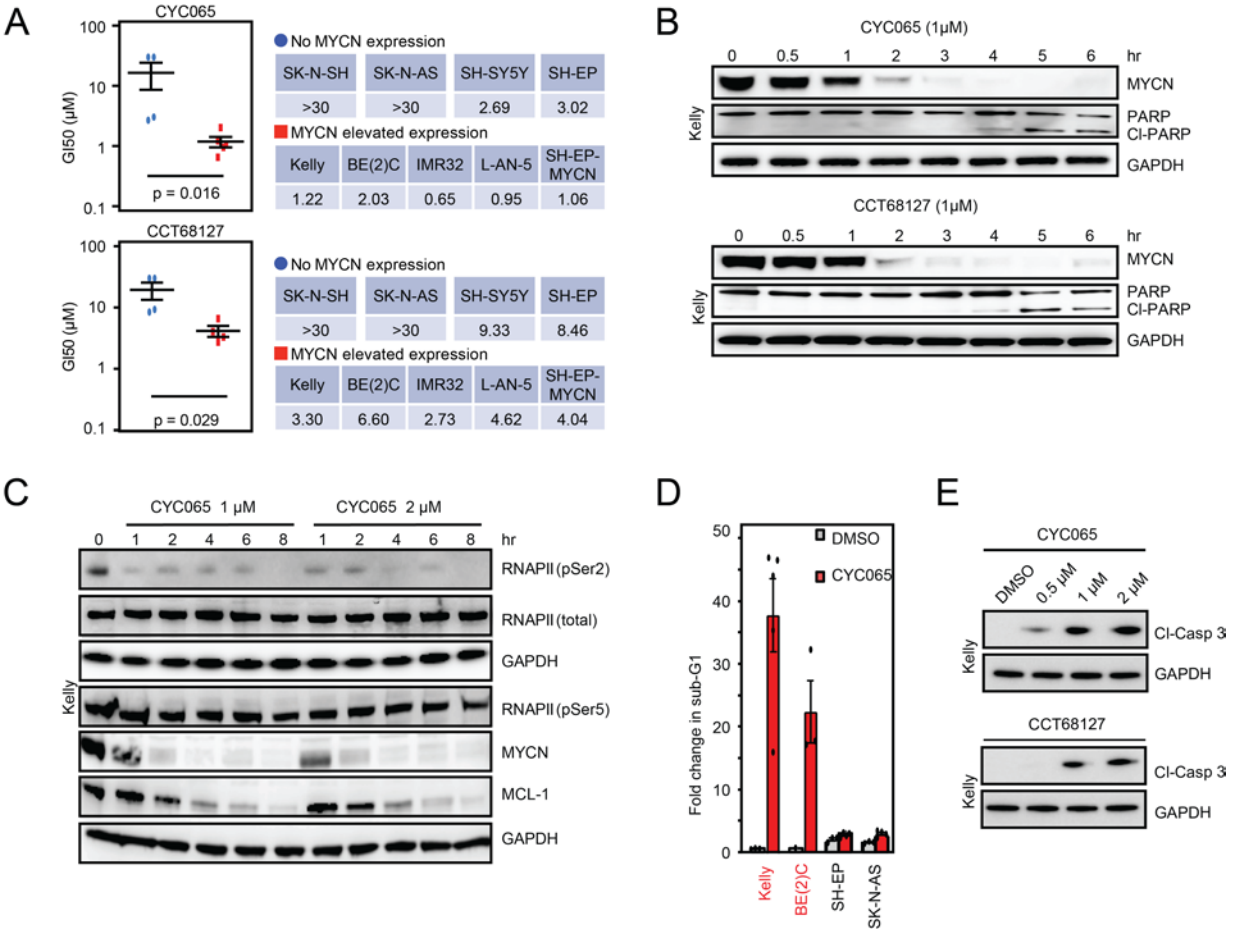
A
CYC065
GI50 (μM)
100
10
1
0.1
p = 0.016
No MYCN expression
SK-N-SH >30
SK-N-AS >30
SH-SY5Y 2.69
SH-EP 3.02
MYCN elevated expression
Kelly 1.22
BE(2)C 2.03
IMR32 0.65
L-AN-5 0.95
SH-EP-MYCN 1.06
CCT68127
p = 0.029
No MYCN expression
SK-N-SH >30
SK-N-AS >30
SH-SY5Y 9.33
SH-EP 8.46
MYCN elevated expression
Kelly 3.30
BE(2)C 6.60
IMR32 2.73
L-AN-5 4.62
SH-EP-MYCN 4.04
B
CYC065 (1μM)
0 0.5 1 2 3 4 5 6 hr
Kelly
MYCN
PARP
Cl-PARP
GAPDH
CCT68127 (1μM)
0 0.5 1 2 3 4 5 6 hr
Kelly
MYCN
PARP
Cl-PARP
GAPDH
C
CYC065 1 μM
CYC065 2 μM
0 1 2 4 6 8 1 2 4 6 8 hr
Kelly
RNAPII (pSer2)
RNAPII (total)
GAPDH
RNAPII (pSer5)
MYCN
MCL-1
GAPDH
D
DMSO
CYC065
Fold change in sub-G1
50
40
30
20
10
0
Kelly
BE(2)C
SH-EP
SK-N-AS
E
CYC065
DMSO
0.5 μM
1 μM
2 μM
Kelly
Cl-Casp 3
GAPDH
CCT68127
Kelly
Cl-Casp 3
GAPDH

822

Figure 1: CDK9 and CDK2 are selectively essential for *MYCN*-amplified neuroblastoma.

A, GI50 of CCT68127 and CYC065 in a panel of NB cells. Cells were treated for 8hr, washed off and replaced with normal growth medium. GI50 values(µM) were calculated after 72hr(n=3). Significance was calculated using two-tailed unpaired Student's t-test.

B, Kelly cells were treated with CYC065 or CCT68127 for 0.5-6hr(1µM). Immunoblots illustrate expression of PARP cleavage(n=2).

C, Immunoblots showing expression of p-RNAPII-Ser2 and -Ser5, MYCN and MCL-1 at the indicated time after treatment with CYC065 (1-2µM, 1-8hr) in Kelly cells(n=2).

D, Flow cytometry analysis showing sub-G1 level of *MYCN*-amplified (Kelly, BE(2)C) and non-amplified (SH-EP, SK-N-AS) cells in response to CYC065 or CCT68127(1µM; 8hr) (+/-S.D. of three independent experiments.

E, Kelly cells were treated with CYC065 or CCT68127 at the indicated concentrations (0.5-2µM) for 6hr. Immunoblots depict expression of cleaved caspase 3(n=2).

Figure 2

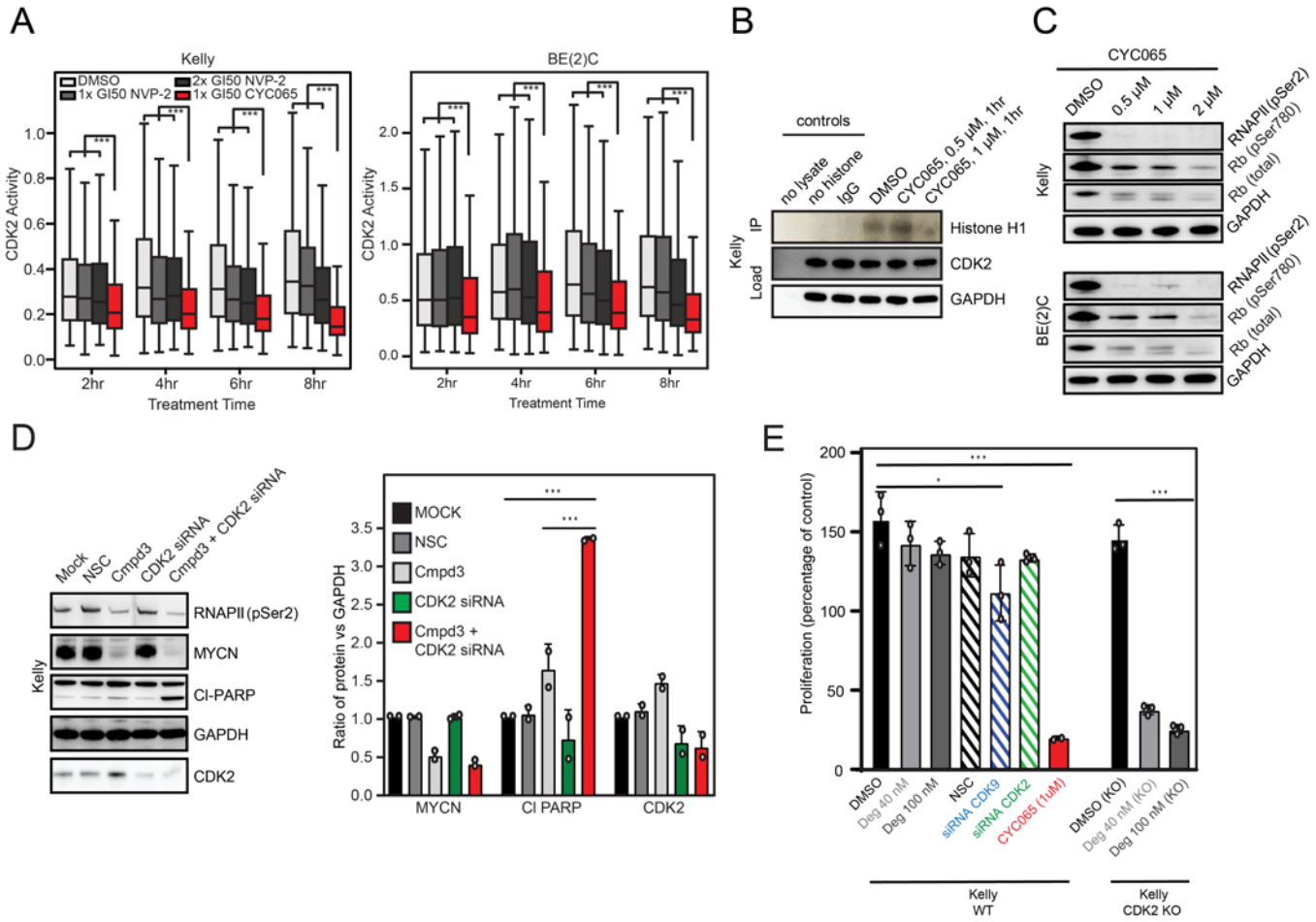
A
Kelly
BE(2)C
DMSO
1x GI50 NVP-2
2x GI50 NVP-2
1x GI50 CYC065
CDK2 Activity
Treatment Time
2hr
4hr
6hr
8hr
B
controls
no lysate
no histone
IgG
DMSO
CYC065, 0.5 μM, 1hr
CYC065, 1 μM, 1hr
Kelly
IP
Load
Histone H1
CDK2
GAPDH
C
CYC065
DMSO
0.5 μM
1 μM
2 μM
Kelly
BE(2)C
RNAPII(pSer2)
Rb (pSer780)
Rb (total)
GAPDH
D
Mock
NSC
Cmpd3
CDK2 siRNA
Cmpd3 + CDK2 siRNA
Kelly
RNAPII (pSer2)
MYCN
Cl-PARP
GAPDH
CDK2
MOCK
NSC
Cmpd3
CDK2 siRNA
Cmpd3 + CDK2 siRNA
Ratio of protein vs GAPDH
MYCN
Cl PARP
CDK2
E
Proliferation (percentage of control)
DMSO
Deg 40 nM
Deg 100 nM
NSC
siRNA CDK9
siRNA CDK2
CYC065 (1uM)
DMSO (KO)
Deg 40 nM (KO)
Deg 100 nM (KO)
Kelly WT
Kelly CDK2 KO

836

Figure 2: CDK9 and CDK2 synergistically maintain *MYCN*-amplified neuroblastoma cells.

A, CDK2 activity is obtained by measuring the cytoplasmic to nuclear ratio of DHB-mVenus. Cell nuclei were identified using DAPI staining. Bold line represents median, box represents the interquartile range (IQR), whiskers represent 1.5 times the IQR, and outliers are not shown. Significance is indicated (Welch's two-tailed t test with Benjamini and Hochberg correction for multiple comparison; ***$P<1x10^{-8}$).

B, Kelly cells were treated with CYC065 or DMSO and harvested after 1hr. CDK2 complexes were immunoprecipitated from cell lysates followed by an in vitro kinase assay using histone H1 as a substrate(n=2).

C, Kelly and BE(2)C cells were treated with CYC065 for the indicated concentrations (0.5-2µM) for 8hr. Immunoblots show expression of the Rb protein(n=2).

D, Immunoblots and bar plots showing expression of MYCN and cleaved PARP when cells were treated with Compound 3 (Cmpd 3) at 1xGI50 and/or siRNA directed to CDK2 (+/-S.D. of two independent experiments; two-tailed unpaired Student's t-test with Benjamini and Hochberg correction for multiple comparison; *P<0.05; **P<0.01; ***P<0.001).

E, Proliferation of NB cells quantified using a Cell-titerGlo assay. Kelly cells with CRISPR Cas9-mediated knockout of CDK2 (KO) or endogenous (WT) CDK2 were treated with CYC065 (8hr), Deg (THAL-SNS-032, 8hr) and siRNA against CDK9 or CDK2 for 48hr (+/-S.D. of three independent experiments, two-tailed unpaired Student's t-test with Benjamini and Hochberg correction for multiple comparison; *P<0.05; **P<0.01; ***P<0.001).

856

Figure 3: Inhibition of CDK9 blocks transcription of *MYCN* and genes with short half-lives.

A-B, Immunoblot and graph showing effects of treatment with CYC065(6hr) on phosphorylation of RNAPII at Ser2 and Ser5 at the indicated concentrations in Kelly cells (+/-S.D. of three independent experiments, two-tailed unpaired Student's t-test with Benjamini and Hochberg correction for multiple comparison; ***P<0.001).

C-D, Click-IT™ assay showing effect of CYC065 or CCT68127 (0.25-1µM, 1hr) on the abundance of newly synthesized nascent RNA in Kelly cells as illustrated in in green fluorescence (C) and the graph (D) (+/-S.D. of four independent experiments, two-tailed unpaired Student's t-test with Benjamini and Hochberg correction for multiple comparison; ***P<0.001). Scale bar: 10µm.

E, Immunofluorescence showing newly synthesized nascent RNA(green) as described in **c**, and FISH of MYCN gene (red) and DAPI-stained nucleus (blue) following 1hr treatment with CYC065 in Kelly cells(n=3). Scale bar: 2µm.

F, Immunoblot showing level of H3K27ac after treatment with CYC065(1µM) for 1hr and 6hr(n=1).

G, Quantitative PCR analyses showing the level of MYCN and MCL-1 genes extracted from the fluorescently labelled nascent RNA in **Figure 3C**(+/-S.D. of four independent experiments, two-tailed unpaired Student's t-test with Benjamini and Hochberg correction for multiple comparison; ***P<0.001).

H, Box plot documenting gene expression changes after CYC065 treatment(1µM, 1hr) of genes with short(<5hr, n=386) and long(>18hr, n=380) mRNA half lifes(60) (two-tailed unpaired Wilcoxon rank sum test).

I, Gene set enrichment analysis in *MYCN*-amplified(Kelly, BE(2)C), *MYCN* non-amplified(SK-N-AS, SH-SY5Y) NB cell lines and tumors from TH-*MYCN* mice after treatment with CYC065. Shown is the "MYC target gene V2" gene set from the Hallmark collection of the MSigDB.

Figure 4

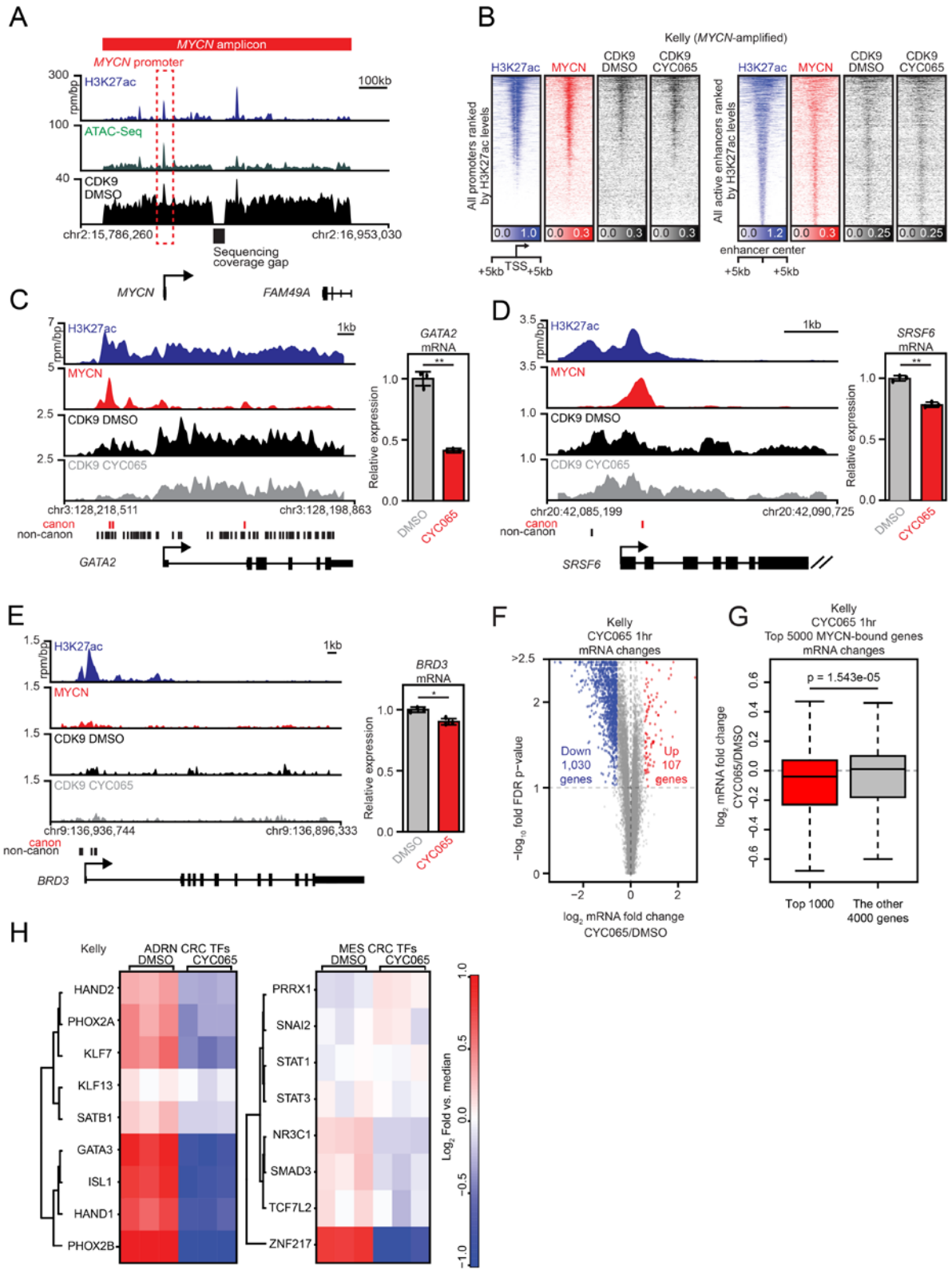
A
MYCN amplicon
MYCN promoter
H3K27ac
ATAC-Seq
CDK9 DMSO
100kb
chr2:15,786,260
chr2:16,953,030
Sequencing coverage gap
MYCN
FAM49A
B
Kelly (MYCN-amplified)
H3K27ac
MYCN
CDK9 DMSO
CDK9 CYC065
All promoters ranked by H3K27ac levels
All active enhancers ranked by H3K27ac levels
TSS
enhancer center
C
GATA2
GATA2 mRNA
Relative expression
DMSO
CYC065
D
SRSF6
SRSF6 mRNA
E
BRD3
BRD3 mRNA
F
Kelly
CYC065 1hr
mRNA changes
Down 1,030 genes
Up 107 genes
log2 mRNA fold change CYC065/DMSO
G
Top 5000 MYCN-bound genes
p = 1.543e-05
Top 1000
The other 4000 genes
H
ADRN CRC TFs
MES CRC TFs
HAND2
PHOX2A
KLF7
KLF13
SATB1
GATA3
ISL1
HAND1
PHOX2B
PRRX1
SNAI2
STAT1
STAT3
NR3C1
SMAD3
TCF7L2
ZNF217
Log2 Fold vs. median

879

Figure 4: Pharmacologic blockade of CDK9 targets the MYCN-dependent transcriptional landscape.

A, Gene tracks of chromatin accessibility(shown by ATAC-Seq, green), active chromatin marker: H3K27ac(blue) and CDK9(black) occupancy at *MYCN* amplicon in Kelly cells.

B, Heatmaps of H3K27ac(blue), MYCN(red), and CDK9(black) occupancy at all promoters(left) or enhancers(right) ranked by H3K27ac signal. Each row of heatmaps suggests one promoter region or enhancer region. The middle of heatmaps indicates the transcription start sites(TSS) or enhancer centers.

C-E, Left: gene tracks of H3K27ac(blue), MYCN(red), and CDK9(black) (+/-CYC065) occupancy at individual loci. ChIP-Seq occupancy is provided in units of reads per million per base pair(rpm/bp). Canonical MYCN binding sites(red lines) and non-canonical MYCN binding sites(black lines) are indicated below gene tracks. Right: bar plots of corresponding gene expression normalized to control showing effect of CYC065(1μM; 1hr) treatment (+/-S.D., two-tailed student t test: *P<0.05, **P<0.01).

F, Scatter plot of log2 gene expression (FPKM) fold changes (CYC065; 1μM; 1hr) treatment vs. DMSO control (x-axis) versus significance of the change (y-axis, -log10 FDR value). Genes with >=1.5-fold change in expression at an FDR<=0.1 are considered differentially expressed(blue and red).

G, The top 5,000 transcriptionally active, expressed and MYCN associated genes are ranked by MYCN load (promoter + enhancer MYCN). Box plot implicating the log2 mRNA fold change of the top 1000 genes and the log2 mRNA fold change of the other 4000 genes(two-tailed student t test).

H, Heatmap indicating the mRNA log2 FPKM fold change from the FPKM median of transcription factors in adrenergic(ADRN) and mesenchymal(MES) core regulatory circuitries, with CYC065(1μM; 1hr) treatment in Kelly cells.

Figure 5

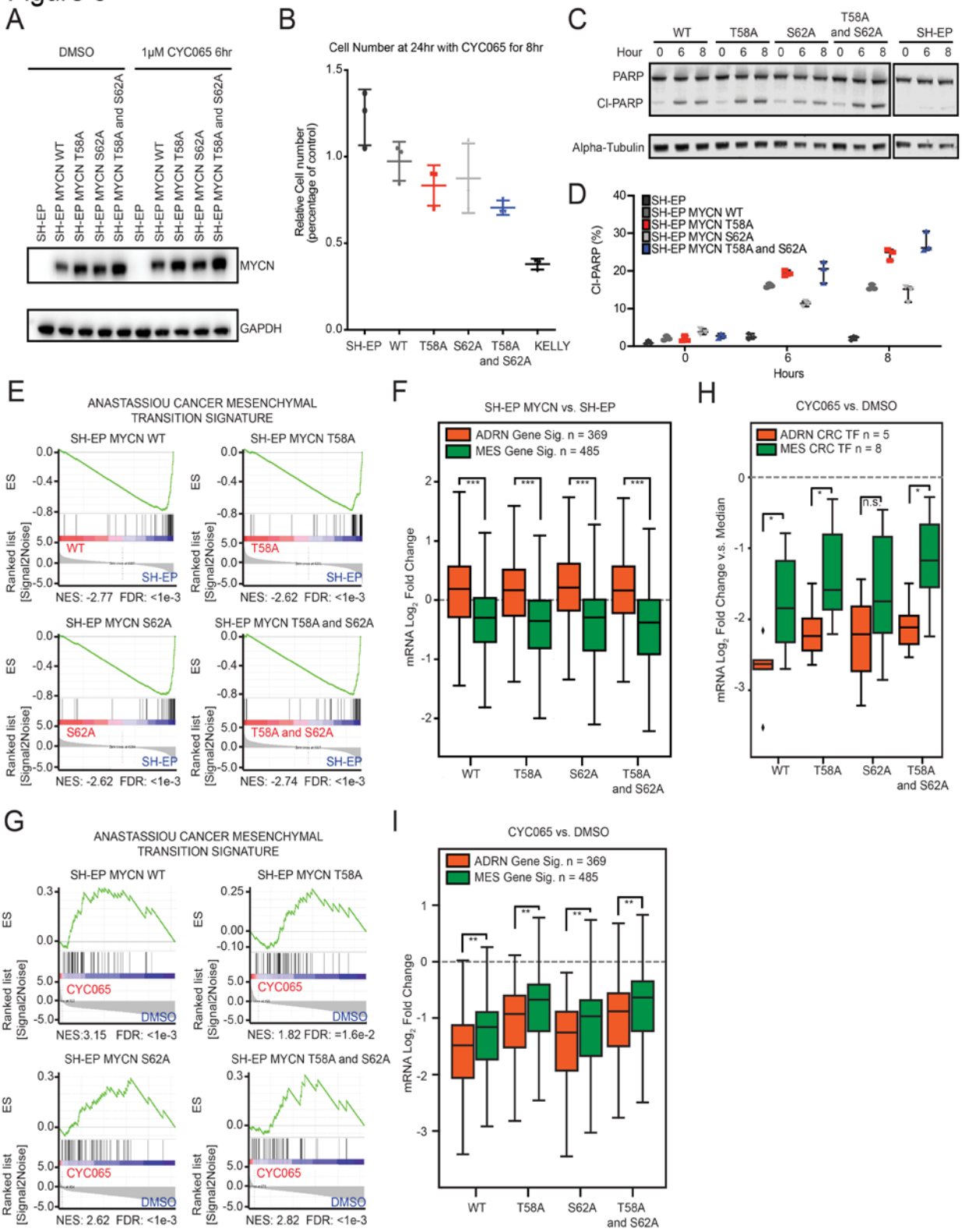
A
DMSO
1μM CYC065 6hr
SH-EP
SH-EP MYCN WT
SH-EP MYCN T58A
SH-EP MYCN S62A
SH-EP MYCN T58A and S62A
MYCN
GAPDH
B
Cell Number at 24hr with CYC065 for 8hr
Relative Cell number (percentage of control)
SH-EP
WT
T58A
S62A
T58A and S62A
KELLY
C
Hour
PARP
Cl-PARP
Alpha-Tubulin
D
Cl-PARP (%)
Hours
E
ANASTASSIOU CANCER MESENCHYMAL TRANSITION SIGNATURE
SH-EP MYCN WT
SH-EP MYCN T58A
SH-EP MYCN S62A
SH-EP MYCN T58A and S62A
ES
Ranked list [Signal2Noise]
NES: -2.77 FDR: <1e-3
NES: -2.62 FDR: <1e-3
NES: -2.62 FDR: <1e-3
NES: -2.74 FDR: <1e-3
F
SH-EP MYCN vs. SH-EP
ADRN Gene Sig. n = 369
MES Gene Sig. n = 485
mRNA Log2 Fold Change
H
CYC065 vs. DMSO
ADRN CRC TF n = 5
MES CRC TF n = 8
mRNA Log2 Fold Change v.s. Median
n.s.
G
ANASTASSIOU CANCER MESENCHYMAL TRANSITION SIGNATURE
CYC065
DMSO
NES:3.15 FDR: <1e-3
NES: 1.82 FDR: =1.6e-2
NES: 2.62 FDR: <1e-3
NES: 2.82 FDR: <1e-3
I
CYC065 vs. DMSO
ADRN Gene Sig. n = 369
MES Gene Sig. n = 485
mRNA Log2 Fold Change

900

Figure 5: CYC065 directly blocks MYCN-driven adrenergic cell identity.

A, Immunoblots indicate stable MYCN expression in SH-EP MYCN system with CYC065 treatment(1μM; 6hr).

B, Potency against SH-EP and SH-EP MYCN cells in vitro. Cells are treated with 1μM CYC065 for 8hr followed by twice PBS washes. Relative cell counts were calculated using Cell-titerGlo assays(+/-S.D. of three independent experiments).

C, Immunoblots depict effect of 1μM CYC065 treatment in SH-EP and SH-EP MYCN cells for 6hr and 8hr.

D, Dot plot showing the quantification of PARP and cleaved PARP (Cl-PARP) in **C.**(+/-S.D. of three independent experiments).

E, Gene set enrichment analysis in SH-EP and SH-EP MYCN cell lines. “Anastassiou Cancer Mesenchymal Transition Signature” is from the Hallmark collection of the Molecular Signatures Database.

F, Box plot showing SH-EP MYCN mRNA $\log_2$ fold change of adrenergic(ADRN) genes and mesenchymal(MES) genes comparing with SH-EP cells. Bold line represents median, box represents the interquartile range(IQR), whiskers represent 1.5 times the IQR. Outliers are not shown. Welch’s two-tailed t test, Benjamini and Hochberg correction for multiple comparison; ***$P<1x10^{-8}$.

G, Gene set enrichment analysis in SH-EP and SH-EP MYCN cell lines after treatments with CYC065(1μM; 6hr).

H, Box plot showing with CYC065(1uM, 6hr), SH-EP MYCN mRNA $\log_2$ fold change of transcription factors from median in adrenergic and mesenchymal core regulatory circuitries. Outliers are represented as dots. Welch’s two-tailed t test and Benjamini and Hochberg correction for multiple comparison; *$P<0.05$

I, Box plot showing with CYC065(1μM; 6hr) treatment, SH-EP MYCN mRNA $\log_2$ fold change of adrenergic(NB ADRN) genes and mesenchymal(NB MES) genes. Outliers are not shown. Welch’s two-tailed t test, Benjamini and Hochberg correction for multiple comparison; **$P<1x10^{-4}$.

Figure 6

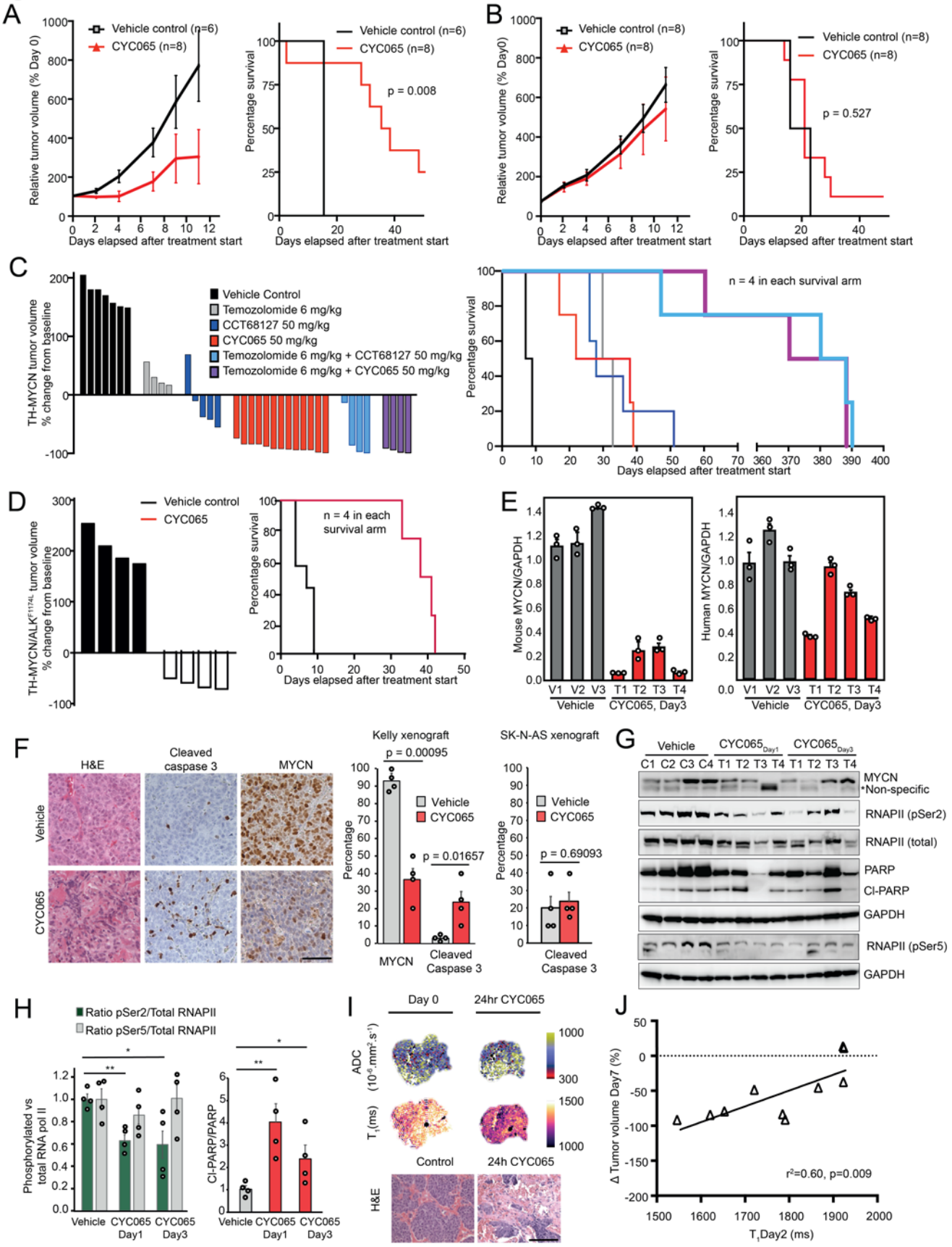
A
Vehicle control (n=6)
CYC065 (n=8)
Relative tumor volume (% Day 0)
Days elapsed after treatment start
Percentage survival
p = 0.008
B
Vehicle control (n=8)
CYC065 (n=8)
Relative tumor volume (% Day0)
p = 0.527
C
Vehicle Control
Temozolomide 6 mg/kg
CCT68127 50 mg/kg
CYC065 50 mg/kg
Temozolomide 6 mg/kg + CCT68127 50 mg/kg
Temozolomide 6 mg/kg + CYC065 50 mg/kg
TH-MYCN tumor volume % change from baseline
n = 4 in each survival arm
D
Vehicle control
CYC065
TH-MYCN/ALK F1174L tumor volume % change from baseline
n = 4 in each survival arm
E
Mouse MYCN/GAPDH
Human MYCN/GAPDH
V1 V2 V3 T1 T2 T3 T4
Vehicle
CYC065, Day3
F
H&E
Cleaved caspase 3
MYCN
Vehicle
CYC065
Kelly xenograft
SK-N-AS xenograft
p = 0.00095
p = 0.01657
p = 0.69093
Percentage
MYCN
Cleaved Caspase 3
G
Vehicle
CYC065Day1
CYC065Day3
C1 C2 C3 C4 T1 T2 T3 T4 T1 T2 T3 T4
MYCN
*Non-specific
RNAPII (pSer2)
RNAPII (total)
PARP
Cl-PARP
GAPDH
RNAPII (pSer5)
GAPDH
H
Ratio pSer2/Total RNAPII
Ratio pSer5/Total RNAPII
Phosphorylated vs total RNA pol II
Cl-PARP/PARP
Vehicle
CYC065 Day1
CYC065 Day3
I
Day 0
24hr CYC065
ADC (10-6.mm2.s-1)
T1(ms)
Control
24h CYC065
H&E
J
Δ Tumor volume Day7 (%)
r2=0.60, p=0.009
T1Day2 (ms)

924

Figure 6: CYC065 and CCT68127 inhibit MYCN-driven neuroblastoma in vivo

Effects of CYC065 on the growth and survival of Kelly(*MYCN*-amplified) (**A**) and SK-N-AS(non-amplified) (**B**) NB xenografts in mice. Data are expressed mean S.E.M(p, Log-Rank Mantel-Cox test with a 5% level of significance).

C, Waterfall plot documenting relative changes in tumor volume at Day 7 in the TH-*MYCN* GEM model. All treatment arms versus control: p<0.001(two-tailed unpaired Student's t-test incorporating a Bonferroni correction(n=5) with a 1% level of significance). Kaplan-Meier plot documenting survival of TH-*MYCN* mice; all treatment arms versus control: p<0.01 and CYC065 or CCT68127 alone versus combination with Temozolomide: p=0.02 (Log-Rank Mantel-Cox test with a 5% level of significance).

D, Waterfall plot documenting relative changes in tumor volume at Day 7 in the TH-ALK^{F1174L}/*MYCN* GEM model (p<0.001, two-tailed unpaired Student's t-test with a 5% level of significance), Kaplan-Meier plot documenting survival of TH-ALK^{F1174L}/*MYCN* mice(p<0.01, Log-Rank Mantel-Cox test with a 5% level of significance).

E, Quantitative RT-PCR analyses showing the level of murine and human *MYCN* RNA in the TH-ALK^{F1174L}/*MYCN* tumor following treatment with CYC065 for 3 days(n=3).

F, Representative images and quantitative analysis of H&E and immunohistochemical staining for cleaved capsase 3 and MYCN in the harvested tumors from **a**. and **b**. Scale bar: 50µm.

G-H, Immunoblot analyses of individual tumors from the TH-*MYCN* model treated with CYC065 for 1 or 3 days(+/-S.D. of four independent experiments, two-tailed unpaired Student's t-test with Benjamini and Hochberg correction for multiple comparison; *P<0.05; **P<0.01).

I, Parametric functional MRI maps showing a reduction of the tumor spin lattice relaxation time T_1 and an increase in the apparent diffusion coefficient (ADC) 24hr after treatment with 50mg/kg CYC065, and their corresponding haematoxylin and eosin staining. Scale bar:100µm.

J, Correlation between native tumor T_1 measured 24hr post treatment with 50mg/kg CYC065 or CCT68127 (% of pretreatment value) and relative changes in tumor volume following treatment with 50mg/kg CYC065.

Gene	Species	Catalogue Number	Company
MYCN	human	Hs00232074	Applied BioSystem
MYCN	mouse	Mm00627179_m1	Applied BioSystem
GAPDH	human	Hs02758991	Applied BioSystem
GAPDH	mouse	Mm03302249	Applied BioSystem
MDM2	human	Hs00242813_m1	Applied BioSystem
ODC1	human	Hs00159739	Applied BioSystem
MCL-1	human	Hs01050896	Applied BioSystem

Table 1: Taqman assays.

Antibody	Catalogue number	Source	Application
MYCN	OP13	Merck	WB, IF
MYCN	Ab-16898	Abcam	ChIP
MYCN	sc-791(rabbit)	Insight Biotechnologies	IP, ChIP
MYCN(pT58)	Ab-28842	Abcam	WB
MYCN(pS62)	Ab-51156	Abcam	WB
MCL-1	sc-819	Insight Biotechnologies	WB
GAPDH	2118L	New England Biolabs	WB
BAX	2772	New England Biolabs	WB
Bad	9292	New England Biolabs	WB
PARP	9542	New England Biolabs	WB
cl-parp	9541	New England Biolabs	WB
caspase-3	9662	New England Biolabs	WB
cl casp3	9661	New England Biolabs	IHC
p53	Ab-8	Thermo Scientific Fisher	WB
p-p53 Ser15	9284	New England Biolabs	WB
p- RNAPII-Ser2	MMS-129R-200	Covance	WB
p- RNAPII-Ser5	MMS-134R-200	Covance	WB

RNApolII	MMS-126R-500	Covance	WB
CDK9	2316	Cell Signaling Technology	WB
Cyclin T1	2098	Abcam	WB
Rb	9313	Cell Signaling Technology	WB
P-Rb-Ser780	9307	Cell Signaling Technology	WB
CDK7	2916	Cell Signaling Technology	WB
H3K27ac	Ab-4729	Abcam	WB
H3K27ac	8173S	Cell Signaling Technology	ChIP
H3	Ab-9715S	Abcam	WB
Actin	AC-15	Abcam	WB

Table 2: Antibodies information. WB: Western blot, IF: Immunofluorescence, IP: Immunoprecipitation, ChIP: Chromatin immunoprecipitation, IHC: Immunohistochemistry.

shRNA	Catalogue number	Details
Cdk9 (1)	TRCN0000000495	AGGGACATGAAGGCTGCTAAT
Cdk9 (2)	TRCN0000199780	GACGTCCATGTTCGAGTACTT
Cdk7 (1)	TRCN0000000592	GCTGTAGAAGTGAGTTTGTAA
Cdk7 (2)	TRCN0000000593	GCAGGAGACGACTTACTAGAT
SHC002	SHC002 MISSION pLKO.1-puro Non-Mammalian shRNA Control	CAACAAGATGAAGAGCACCAA

Table 3: shRNA from TRC library (Sigma Aldrich, U.K.).

Exon	PCR Primer Forward	PCR Primer Reverse	Size (bp)
5-6	tgttcacttgtgccctgact	ttaacccctcctcccagaga	467
7	cttgccacaggtctccccaa	aggggtcagaggcaagcaga	237
8-9	ttgggagtagatggagcct	agtgttagactggaaacttt	445

Table 4: Primers used for testing the TP53 mutation status.

Sample name	Mapped reads	Mapped %	PCR cycles	Peaks	GEO series	GEO accession
KELLY_CYC065_CDK9	41464643	96.89	12	1624	GSE107126	GSM2861546
KELLY_CYC065_H3K27AC	39901878	96.6	10	12421	GSE107126	GSM2861545
KELLY_CYC065_WCE	43932669	97.48	8	NA	GSE107126	GSM2861542
KELLY_DMSO_CDK9	43875937	96.27	13	1940	GSE107126	GSM2861544
KELLY_DMSO_H3K27AC	45167019	96.5	11	13215	GSE107126	GSM2861543
KELLY_DMSO_WCE	49526849	97.54	8	NA	GSE107126	GSM2861541
KELLY_MYCN	59487674	97.54	5	7074	GSE80151	GSM2113526
KELLY_WCE	44532043	92.32	5	NA	GSE80151	GSM2113525
KELLY_H3K27AC	77156218	94.71	5	31429	GSE80151	GSM2113524
SHEP_MYCN_WT_DMSO_MYCN	32072864	81.1	11	17452	GSE128330	GSM3671495
SHEP_MYCN_WT_CYC065_MYCN	34010613	80.47	12	18566	GSE128330	GSM3671496
SHEP_MYCN_T58A_DMSO_MYCN	33026439	80.58	11	12174	GSE128330	GSM3671497
SHEP_MYCN_T58A_CYC065_MYCN	29785344	81.29	12	12560	GSE128330	GSM3671498
SHEP_MYCN_S62A_DMSO_MYCN	30368111	80.55	12	13636	GSE128330	GSM3671499
SHEP_MYCN_S62A_CYC065_MYCN	34846800	80.79	12	17812	GSE128330	GSM3671500
SHEP_MYCN_T58A_and_S62A_DMSO_MYCN	31945930	91.67	13	18056	GSE128330	GSM3671493
SHEP_MYCN_T58A_and_S62A_CYC065_MYCN	22719761	91.56	13	9120	GSE128330	GSM3671494
SHEP_MYCN_WT_DMSO_WCE	34846800	80.79	8	NA	GSE128330	GSM3671501
SHEP_MYCN_WT_CYC065_WCE	26647343	79.58	10	NA	GSE128330	GSM3671506
SHEP_MYCN_T58A_DMSO_WCE	23149810	79.95	10	NA	GSE128330	GSM3671502
SHEP_MYCN_T58A_CYC065_WCE	35848374	80.34	9	NA	GSE128330	GSM3671507
SHEP_MYCN_S62A_DMSO_WCE	31935621	78.09	11	NA	GSE128330	GSM3671503
SHEP_MYCN_S62A_CYC065_WCE	35089754	80.63	10	NA	GSE128330	GSM3671508
SHEP_MYCN_T58A_and_S62A_DMSO_WCE	22139842	91.1	15	NA	GSE128330	GSM3671504
SHEP_MYCN_T58A_and_S62A_CYC065_WCE	25732969	90.63	13	NA	GSE128330	GSM3671509
SHEP_MYCN_WT_DMSO_H3K27AC	23186326	92.04	8	46200	GSE128330	GSM3671483
SHEP_MYCN_WT_CYC065_H3K27AC	26878855	92.12	8	51282	GSE128330	GSM3671484
SHEP_MYCN_T58A_DMSO_H3K27AC	28514145	92	8	43864	GSE128330	GSM3671485
SHEP_MYCN_T58A_CYC065_H3K27AC	26352153	92.6	8	47768	GSE128330	GSM3671486
SHEP_MYCN_S62A_DMSO_H3K27AC	24276534	92.04	8	48365	GSE128330	GSM3671487
SHEP_MYCN_S62A_CYC065_H3K27AC	24271796	92.54	8	50834	GSE128330	GSM3671488

SHEP_MYCN_T58A_and_S62A_DMSO_H3K27AC	24707663	92.54	8	48304	GSE128330	GSM3671489
SHEP_MYCN_T58A_and_S62A_CYC065_H3K27AC	23745960	92.82	9	50624	GSE128330	GSM3671490

Table 5: Sequencing depth of ChIP-Seq experiments.

Cell lines	**Origin**	**Myc status**
Kelly	Neuroblastoma	*MYCN*-amplified
BE(2)C	Neuroblastoma	*MYCN*-amplified
IMR32	Neuroblastoma	*MYCN*-amplified
L-AN-5	Neuroblastoma	*MYCN*-amplified
SK-N-SH	Neuroblastoma	No MYCN expression
SK-N-AS	Neuroblastoma	No MYCN expression
SH-SY5Y	Neuroblastoma	No MYCN expression
SH-EP	Neuroblastoma	No MYCN expression
SH-EP(MYCN WT)	Neuroblastoma	Exogenously-expressed wild-type MYCN protein
SH-EP(MYCN T58A)	Neuroblastoma	Exogenously-expressed MYCN protein mutated at T58A
SH-EP(MYCN S62A)	Neuroblastoma	Exogenously-expressed MYCN protein mutated at S62A
SH-EP(MYCN T58A and S62A)	Neuroblastoma	Exogenously-expressed MYCN protein mutated at T58A and S62A
H128	Lung	No MYC, MYCL or MYCN expression
H510A	Lung	Expressed MYCL protein
H526	Lung	Expressed MYCN protein
COLO-320	Colon	Expressed c-MYC protein
SKBR3	Breast	Expressed c-MYC protein
HCC1954	Breast	Expressed c-MYC protein

Table 6: Genetic characteristics of cell lines.

Sample name	GEO series	GEO accession
SHEP_MYCN_WT_DMSO_1	GSE145068	GSM4305685
SHEP_MYCN_WT_DMSO_2	GSE145068	GSM4305686
SHEP_MYCN_WT_DMSO_3	GSE145068	GSM4305687
SHEP_MYCN_WT_CYC065_1	GSE145068	GSM4305688
SHEP_MYCN_WT_CYC065_2	GSE145068	GSM4305689
SHEP_MYCN_WT_CYC065_3	GSE145068	GSM4305690
SHEP_MYCN_S62A_DMSO_1	GSE145068	GSM4305691
SHEP_MYCN_S62A_DMSO_2	GSE145068	GSM4305692
SHEP_MYCN_S62A_DMSO_3	GSE145068	GSM4305693
SHEP_MYCN_S62A_CYC065_1	GSE145068	GSM4305694
SHEP_MYCN_S62A_ CYC065_2	GSE145068	GSM4305695
SHEP_MYCN_S62A_ CYC065_3	GSE145068	GSM4305696
SHEP_MYCN_T58A_DMSO_1	GSE145068	GSM4305697
SHEP_MYCN_T58A_DMSO_2	GSE145068	GSM4305698
SHEP_MYCN_T58A_DMSO_3	GSE145068	GSM4305699
SHEP_MYCN_T58A_CYC065_1	GSE145068	GSM4305700
SHEP_MYCN_ T58A _ CYC065_2	GSE145068	GSM4305701
SHEP_MYCN_T58A _ CYC065_3	GSE145068	GSM4305702
SHEP_MYCN_T58A_and_S62A_DMSO_1	GSE145068	GSM4305703
SHEP_MYCN_T58A_and_S62A _DMSO_2	GSE145068	GSM4305704
SHEP_MYCN_T58A_and_S62A _DMSO_3	GSE145068	GSM4305705
SHEP_MYCN_T58A_and_S62A _CYC065_1	GSE145068	GSM4305706
SHEP_MYCN_ T58A _and_S62A _ CYC065_2	GSE145068	GSM4305707
SHEP_MYCN_T58A _and_S62A _ CYC065_3	GSE145068	GSM4305708
SHEP _DMSO_1	GSE145068	GSM4305709
SHEP_DMSO_2	GSE145068	GSM4305710
SHEP_ DMSO_3	GSE145068	GSM4305711

SHEP_ CYC065_1	GSE145068	GSM4305712
SHEP_ CYC065_2	GSE145068	GSM4305713
SHEP_ CYC065_3	GSE145068	GSM4305714

Table 7: GEO session information of RNA-Seq experiments.

Supplemental Figure 1

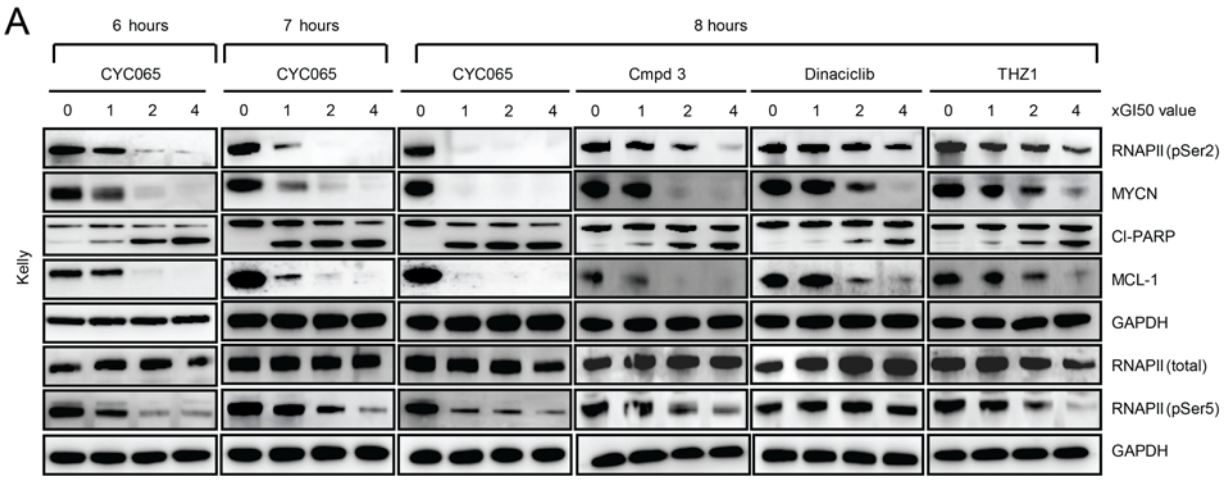

Inhibitor	Selectivity (nM) CDK2	CDK7	CDK9	Others
CYC065	8	612	14	CDK5
CCT68127	10	520	9	CDK5
Compound 3	580		14	
Dinaciclib	1		4	CDK1(3), CDK5(1)
THZ1		3.2		
SNS-032	62	38	4	
Flavopiridol	405	514	11	CDK1(27), CDK4(132)
BAY1143572			13	
Palbociclib				CDK4(11), CDK6(16)

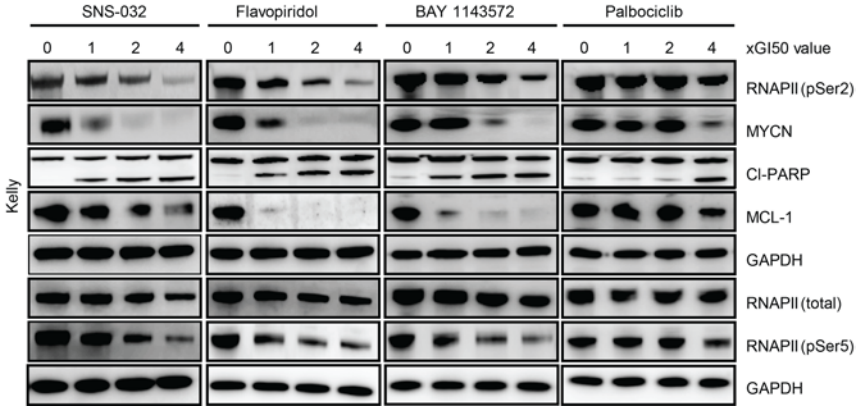

964

Supplemental Figure 1: *MYCN*-amplified neuroblastoma is sensitive to CDK9 inhibitors.

A, Immunoblots depict effects of treatment with CDK inhibitors at the indicated time and concentrations in Kelly cells (n=1-3). Table showing reported selectivity of the CDK inhibitors(16, 26, 27, 50).

Supplemental Figure 2

A

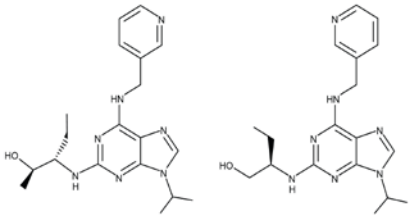

CCT68127 (pre-clinical probe)

seliciclib (CYC202, R-Roscovitine)

B

Inhibitor	GI50 (72 hrs) nM	% Viable cells
CYC202	6250	NT
CCT68127	853	52
CYC065	430	47
Compound 3	80	76
Dinaciclib	3	78
THZ1	30	83
SNS - 032	498	65
Flavopiridol	60	87
BAY1143572	501	83
Palbociclib	4957	81

C

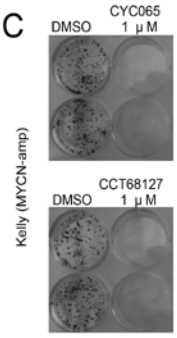

D

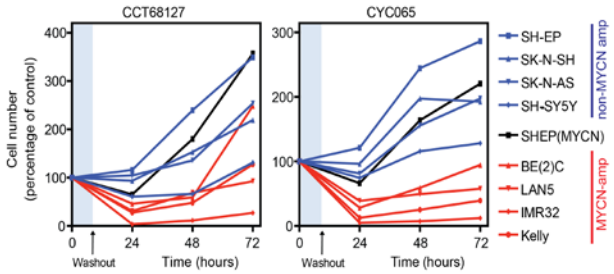

E

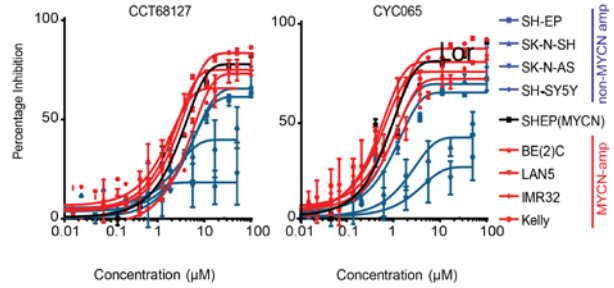

F

		DMSO	CCT68127	CYC065
Kelly	G0/G1	46.9	47.4	45.4
	S	27.9	22.3	27.1
	G2M	23.2	17.1	12
	Sub G1	1.1	12.5	15.1
BE(2)C	G0/G1	45	36.2	31.3
	S	25.3	22.1	24.7
	G2M	27.5	27.9	18.1
	Sub G1	1.4	10.7	23.2
SH-EP	G0/G1	61.3	55.5	53.5
	S	14.8	18.2	21.6
	G2M	21.2	21.2	19.1
	Sub G1	2.2	4.5	4.9
SK-N-AS	G0/G1	45.4	42.7	47.3
	S	24.6	21.5	20.9
	G2M	28.3	33.8	29.4
	Sub G1	0.5	0.8	0.9

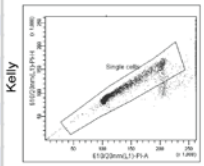

G

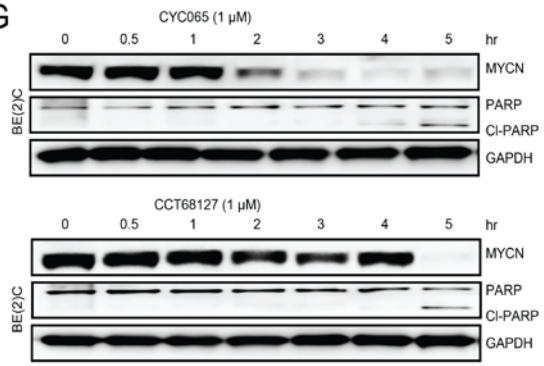

H

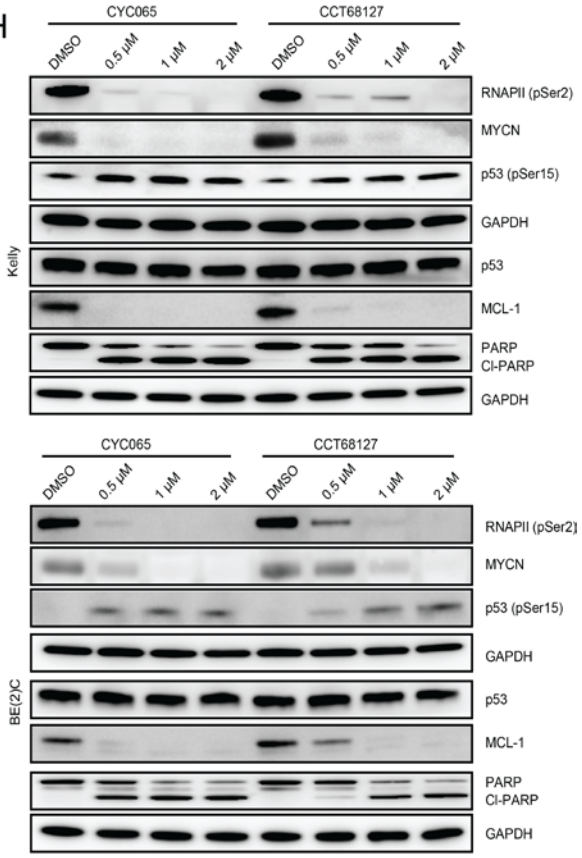

I

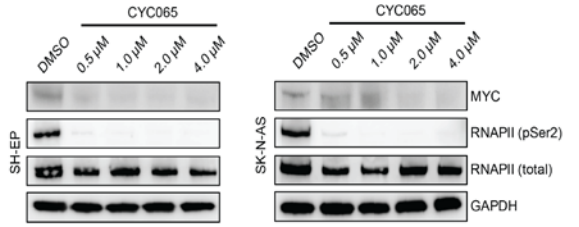

J

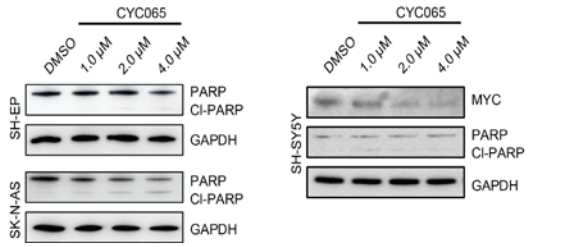

969

Supplemental Figure 2: CYC065 and CCT68127 target MYCN-driven neuroblastoma and induce apoptosis.

A, Structures of CCT68127 and seliciclib (CYC202).

B, GI50 of CCT68127, CYC065, seliciclib (CYC202) and other CDK inhibitors in Kelly NB cells. Cells were treated continuously with each compound for 72 hr and GI50 values (nM) were calculated after 72 hr using an SRB assay (n= 3).

C, Crystal violet-stained culture dishes of Kelly NB cells after treatment with CYC065 or CCT68127 (1 µM, 8hr) or vehicle (DMSO), replated and replaced with normal growth media for 7 days (n=2).

D, Proliferation of NB cells over 72hr quantified using a Cell-titerGlo assay. Cells were treated with CYC065 (1 µM) and CCT68127 (2 µM) for 8hr, washed off and replaced with normal growth medium (n=3).

E, GI50 curve of Figure 1b (n= 3).

F, Flow cytometry analysis showing cell cycle phases of *MYCN*-amplified (Kelly, BE(2)C) and non-*MYCN*-amplified (SH-EP, SK-N-AS) cells in response to CYC065 or CCT68127 (1 µM; 8hr) as indicated in Fig 1e. A pulse geometry gate PI-H x PI-A was used to gate out the doublets and debris (n= 2).

G, BE(2)C cells were treated with CYC065 or CCT68127 at 1 µM for 0.5-5hr. Immunoblots depict expression of MYCN and cleaved PARP (n= 2).

H, Immunoblots depict expression of MYCN, MCL-1, PARP, p53, p-p53 at Ser15 and GAPDH in Kelly and BE(2)C cells following treatment with CYC065 or CCT68127 (0.5-2 µM; 8hr) (n= 2).

I, Immunoblots showing expression of MYC, RNAPII Ser2P and GAPDH in SH-EP and SK-N-AS cells following treatment with CYC065 (0.5-4 µM; 8hr) (n= 2).

J, Immunoblots depict expression of cleaved PARP and GAPDH in SH-EP, SK-N-AS and SH-SY5Y cells following treatment with CYC065 (1-4 µM; 8hr) (n= 2).

Supplemental Figure 3

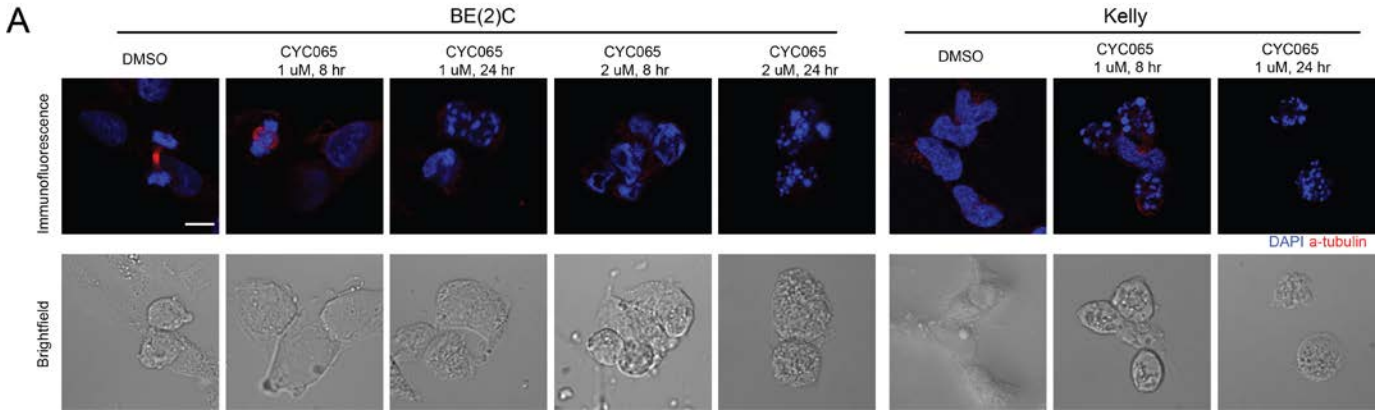

Supplemental Figure 3: CYC065 does not induce anaphase catastrophe in MYCN-driven neuroblastoma.

A, Immunofluorescence and brightfield images documenting morphological changes and staining with α-tubulin (red) and nuclei Dapi (blue) in BE(2)C and Kelly cells after treatment with CYC065 (1-2 µM, 8-24hr). DMSO control cells shows two spindle poles. Multipolar anaphases (multiple spindle poles) was not detected in CYC065 treated cells. Scale bars = 5 µm (n= 3).

Supplemental Figure 4

A

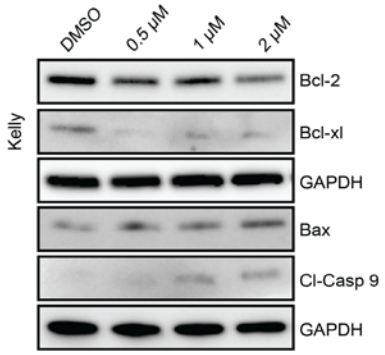

B

Cell line	TP53 status	Protein description
BE(2)C	Mutated	P.C135F
Kelly	Mutated	P.P177T
IMR32	Wild type	
L-AN-5	Wild type	

C

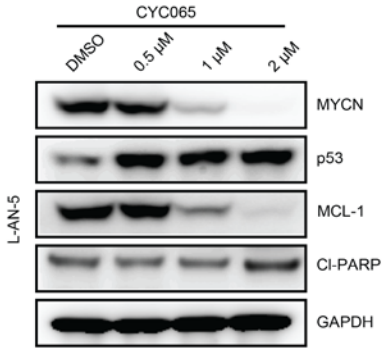

D

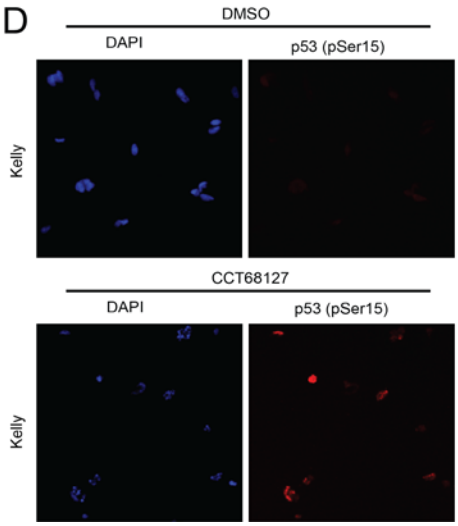

E

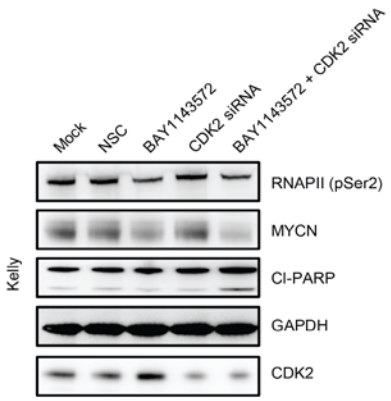

F

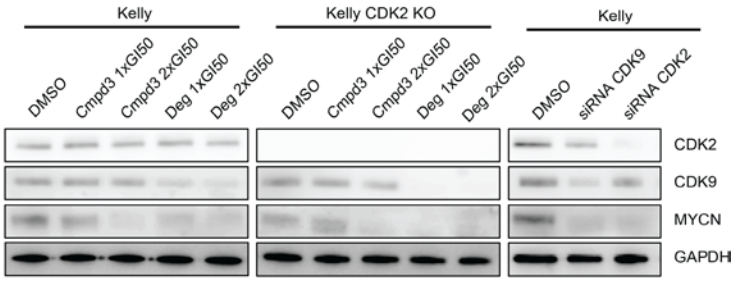

G

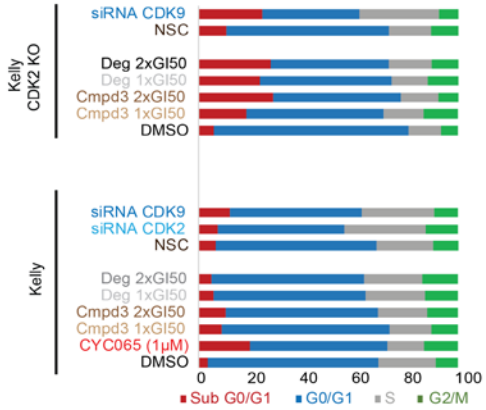

1001

Supplemental Figure 4: CDK9 and CDK2 inhibition induces TP53 mediated apoptosis.

A, Immunoblots showing expression of the indicated proteins and GAPDH in Kelly cells following treatment with CYC065 (0.5-2 µM, 6hr).

B, TP53 mutation status of the tested cells.

C, Immunoblots depict expression of p53, p-p53 at Ser15, MYCN, MCL-1, PARP and GAPDH in p53 native L-AN-5 cells following treatment with CYC065 or CCT68127 at the indicated concentrations for 6hr.

D, Immunofluorescence showing p-p53 at Ser15 (red) in Kelly cells after treatment with CCT68127 for 6hr.

E, Immunoblots depict expression of MYCN, CDK2 and PARP cleavage in Kelly cells after treatment with BAY1143572 (GI50, 6hr), CDK2 siRNA (48hr) or both (pretreatment with CDK2 siRNA for 42hr before treatment with BAY1143572 for a further 6hr).

F, Immunoblots showing expression of MYCN after treatment with Compound 3 (Cmpd3) and CDK9 degrader THAL-SNS-032 (1-2xGI50, 8hr), genetic knockdown of CDK9 or CDK2 by siRNA (48hr) and genetic knockout of CDK2 by CRISPR in Kelly cells.

G, Kelly cell cycle profile after genetic knockdown of CDK9 or CDK2 by siRNA (48hr), genetic knockout of CDK2 by CRISPR and/or treatment with Compound 3 (Cmpd3) and CDK9 degrader THAL-SNS-032 (1-2xGI50, 8hr). GI50 of THAL-SNS-032 is 40 nM.

Supplemental Figure 5

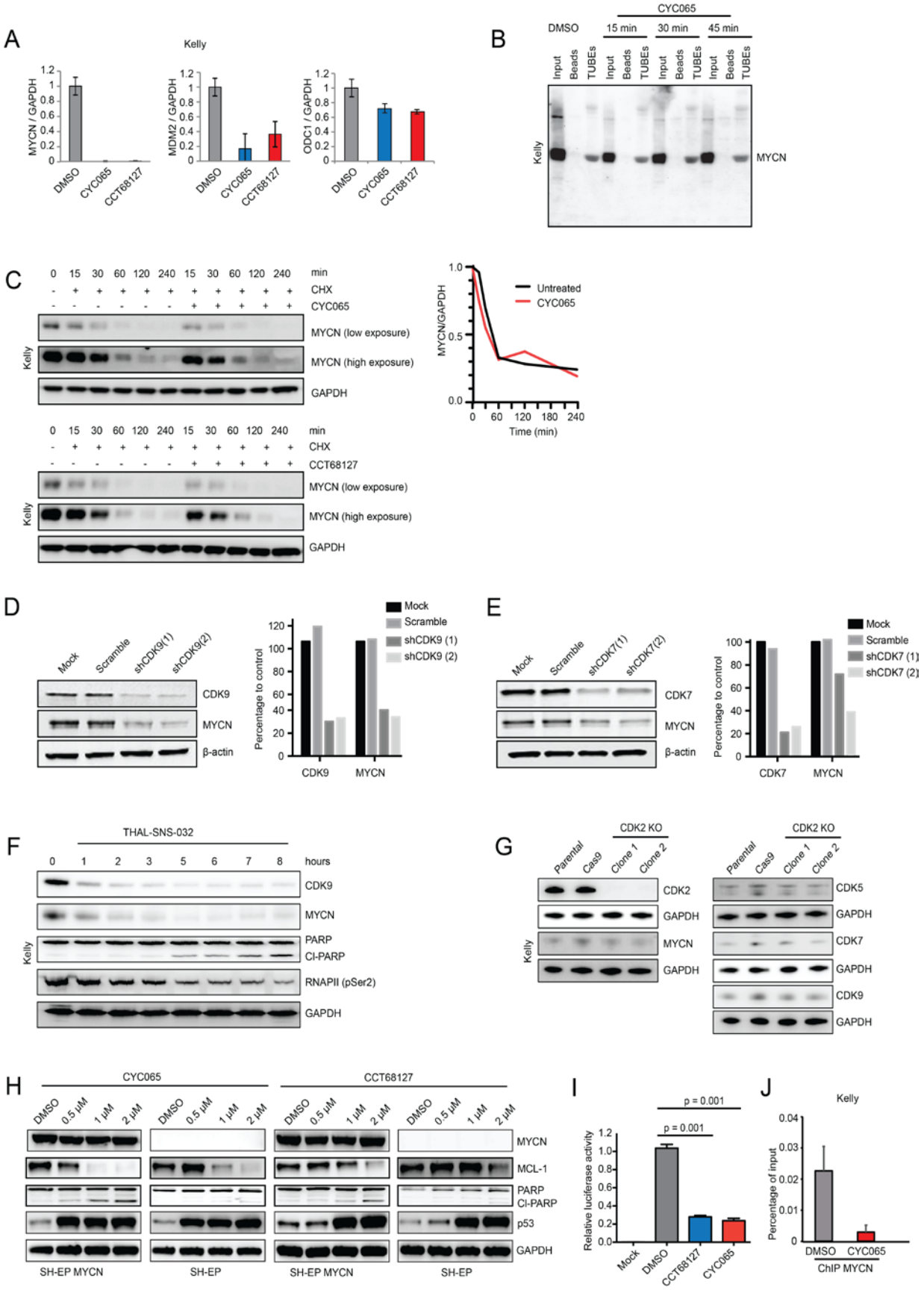

1018

Supplemental Figure 5: Effects of inhibition of CDK9, CDK7 and CDK2 on MYCN protein.

A, Quantitative RT-PCR showing MYCN genes and MYCN target genes, MDM2 and ODC1, after treatment with CYC065 or CCT68127 (1 µM, 8hr) in Kelly NB cells (+/- S.D. of two independent experiments; Significance was calculated using two-tailed unpaired Student's t-test).

B, Tandem Ubiquitin Binding Entity (TUBE) pulldown assay showing no change in ubiquitinated MYCN protein after treatment with CYC065 (1 µM) at the indicated time.

C, BE(2)C cells were treated with CYC065 (1 µM) or CCT68127 (1 µM) and cycloheximide (25 µg/ml), harvested at the indicated time points, and immunoblotted for MYCN protein.

D, Immunoblots and graph showing expression of CDK9 and MYCN proteins when CDK9 is down-regulated by shRNA.

E, Immunoblots and graph showing expression of CDK7 and MYCN proteins when CDK7 is down-regulated by shRNA.

F, Immunoblots showing effect of CDK9 degrader THAL-SNS-032 (0.1 µM, 1-8hr) on CDK9, cleaved PARP, phosphorylated RNAPII Ser2 and MYCN protein levels

G, Immunoblots showing genetic knockout of CDK2 in Kelly cells.

H, Immunoblot showing the effects of CYC065 or CCT68127 (6hr) in native SH-EP cells that lack the native transcriptional machinery of MYCN and SH-EP MYCN WT cells with exogenously-expressed MYCN WT.

I, Cells were transfected with a MYCN promoter Renilla luciferase construct and Cypridina TK control construct, and treated with compounds (1 µM) for 6hr at 48hr post transfection. Luciferase reading was normalized to the Cypridina TK control signal (+/- S.D. of two independent experiments).

J, Results of ChIP assays using MYCN at a genomic region surrounding the E box of the APEX gene after treatment with CYC065 (1 µM, 1hr). (+/- S.D. of three independent experiments).

Supplemental Figure 6

A

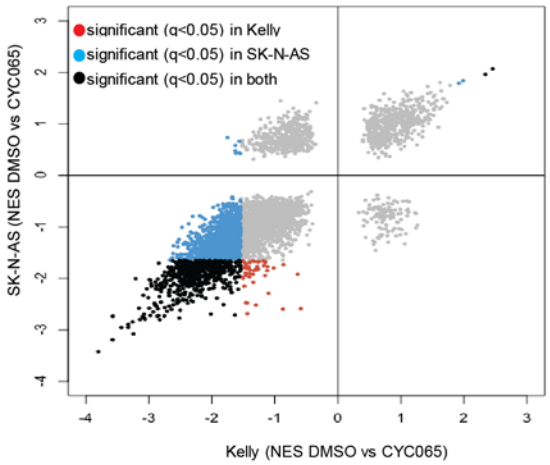

B

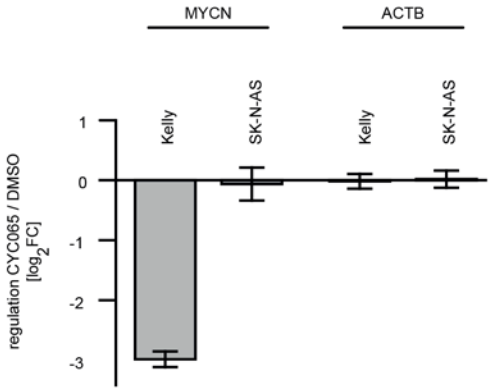

C

gene set	Kelly NES	Kelly q-value	SK-N-AS NES	SK-N-AS q-value
Reactome: Generic transcription pathway	-3.8	<1e-4	-3.4	<1e-4
Reactome: RNA POL II transcription	-2.7	<1e-4	-2.0	2.0e-3
Reactome: RNA POLI, RNA POLIII and mitochondrial transcription	-2.5	<1e-4	-2.8	<1e-4
PID: TRKR pathway	-1.7	<2e-2	-0.7	<1e0

D

gene set	TH-MYCN NES	TH-MYCN q-value
Reactome: Transcription	-2.7	<1e-4
Reactome: RNA POLI, RNA POLIII and mitochondrial transcription	-2.5	<1e-4
Reactome: RNA POL II transcription	-2.5	<1e-4
Rhodes: Undifferentiated cancer	-2.4	<1e-4

E

Gene set	Kelly NES	Kelly FDR	BE(2)C NES	BE(2)C FDR	SK-N-AS NES	SK-N-AS FDR	SH-SY5Y NES	SH-SY5Y FDR	TH-MYCN tumors NES	TH-MYCN tumors FDR
MYC targets V2	-2.46	<1.0e-4	-1.95	<1.0e-4	-1.85	1.72e-3	2.19	<1.0e-4	-1.95	5.20e-4
MYC targets V1	-1.46	2.53e-2	-1.38	6.88e-2	-1.00	5.32e-1	-0.69	1.00e0	-2.90	<1.0e-4
Yu: MYC targets up	-2.31	8.41e-6	-1.58	8.36e-2	-1.45	1.33e-1	-1.63	3.36e-2	-2.73	<1.0e-4
Schlosser: MYC targets and serum response up	-2.23	8.47e-5	-1.68	5.31e-2	-1.78	1.99e-2	-1.62	3.70e-2	-1.66	3.17e-2
Ben-Porath: MYC targets with E-box	-1.93	3.05e-3	-1.62	6.91e-2	-1.57	7.66e-2	-1.47	9.10e-2	-0.79	9.62e-1
Acosta: Proliferation independent MYC targets up	-1.91	3.84e-3	-1.55	9.33e-2	-0.59	1.00e-0	-1.25	2.57e-1	-1.03	5.61e-1
Dang: Regulated by MYC up	-1.89	4.24e-3	-1.25	3.01e-1	-1.00	6.91e-1	-1.30	2.02e-1	-2.33	1.68e-4

1041

Supplemental Figure 6: Gene expression changes upon CYC065 treatment.

A, The xy plot shows overall changes in GSEA after CYC065 treatment (1 µM, 1hr) in Kelly and SK-N-AS cells. Each dot represents one gene set from the MSigDB C2 collection. Significant gene sets with an FDR q-value <0.05 are highlighted.

B, Expression changes of MYCN upon CYC065 treatment in Kelly and SK-N-AS cells used in Affymetrix gene expression array as demonstrated in **c.** Plotted are $\log_2$ fold changes and 95% confidence intervals of 3 biological replicates. B-actin (ACTB) as a not-regulated control.

C, Summary of GSE analyses demonstrate repression of genes after CYC065 treatment in Kelly and SK-N-AS cells.

D, Summary of GSE analyses in CYC065 treated TH-*MYCN* mice.

E, Gene set enrichment analysis in *MYCN*-amplified (Kelly, BE(2)C), *MYCN* non-amplified (SK-N-AS, SH-SY5Y) NB cell lines and tumors from TH-*MYCN* mice after treatment with CYC065. Selected MYC gene sets from the C2 collection of the MSigDB are shown. Gene sets with a non-significant Benjamini-Höchberg-corrected p-value (FDR <0.25) are highlighted in red.

Supplemental Figure 7

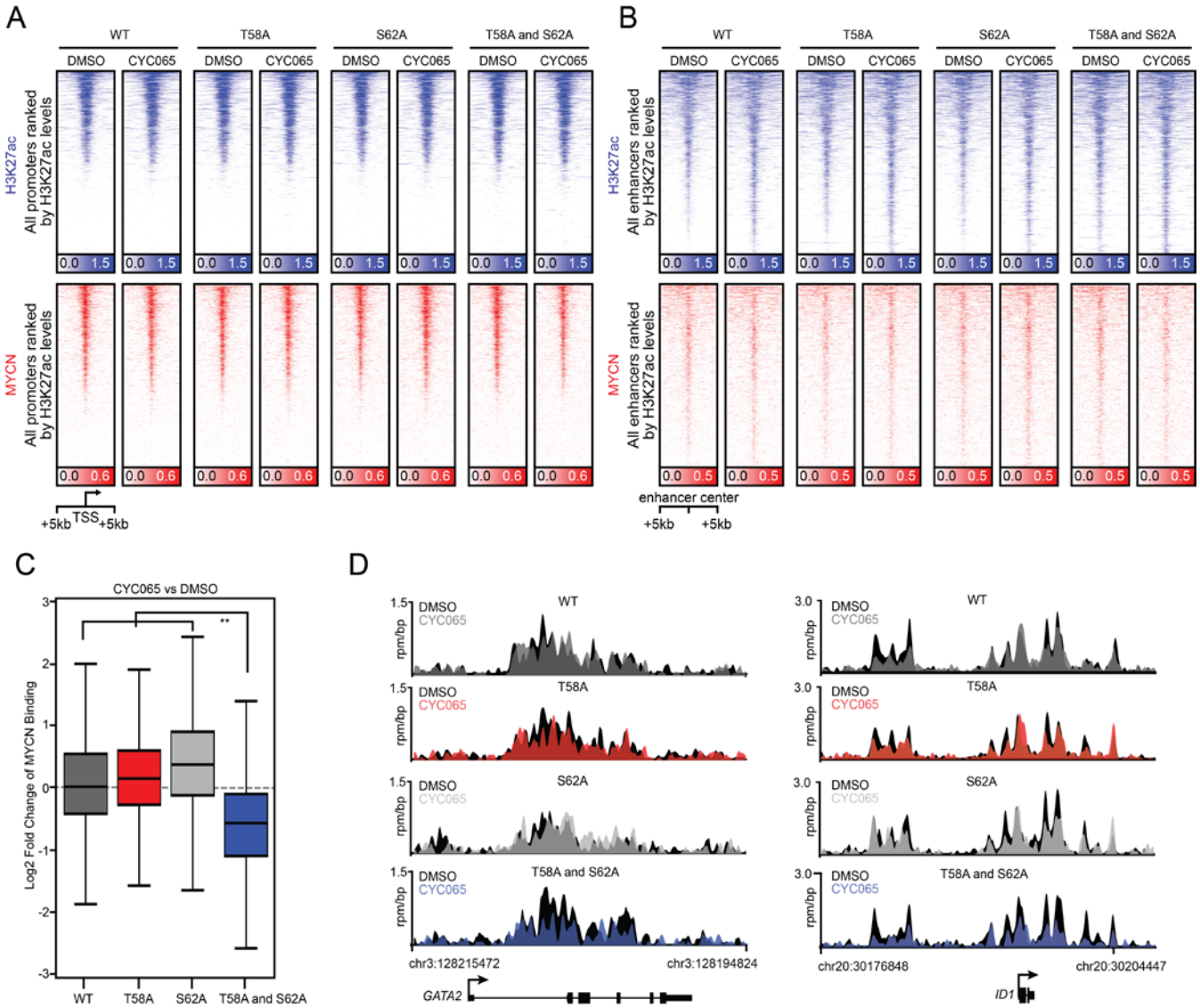

E

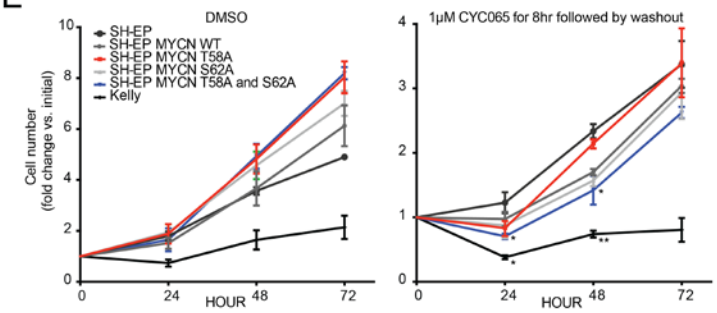

1057

Supplemental Figure 7: CYC065 fails to alter global H3K27ac and MYCN occupancy in SH-EP MYCN lines.

A, Heatmaps of H3K27ac (blue) and MYCN (red) occupancy at all promoters (+/- CYC065, 1 µM, 6hr) treatment ranked by SH-EP MYCN WT DMSO H3K27ac signal.

B, Heatmaps of H3K27ac (blue) and MYCN (red) occupancy at all enhancers (+/- CYC065, 1 µM, 6hr) treatment ranked by SH-EP MYCN WT DMSO H3K27ac signal.

C, Box plot showing the $\log_2$ fold change of genome-wide MYCN occupancy with CYC065 (1 µM, 6hr). Bold line represents median, box represents the interquartile range (IQR), whiskers represent 1.5 times the IQR, and outliers are not shown. Significance is indicated (Welch's two-tailed t test and Benjamini and Hochberg correction): **$P < 1x10^{-8}$ and FDR $< 1x10^{-8}$.

D, Gene tracks MYCN (+/- CYC065, 1 µM, 6hr) occupancy at individual loci. ChIP-Seq occupancy is provided in units of reads per million per base pair (rpm/bp).

E, Proliferation of NB cells over 72hr quantified using a Cell-titerGlo assay. Cells were treated with DMSO or 1 µM CYC065 for 8hr. DMSO or CYC065 treatment were washed off by PBS twice and replaced with normal growth medium (+/- S.D. of three independent experiments). For 24hr, SH-EP vs SH-EP MYCN (T58A), SH-EP vs SH-EP MYCN (T58A and S62A) and SH-EP vs Kelly were statistically significant. For 48hr, SH-EP vs SH-EP MYCN (WT), SH-EP vs SH-EP MYCN (S62A), SH-EP vs SH-EP MYCN (T58A and S62A) and SH-EP vs Kelly were statistically significant. Significance is indicated (two-tailed student t test and Benjamini and Hochberg correction): *$P < 0.05$ and FDR < 0.05, **$P < 1x10^{-4}$ and FDR $< 1x10^{-3}$.

Supplemental Figure 8

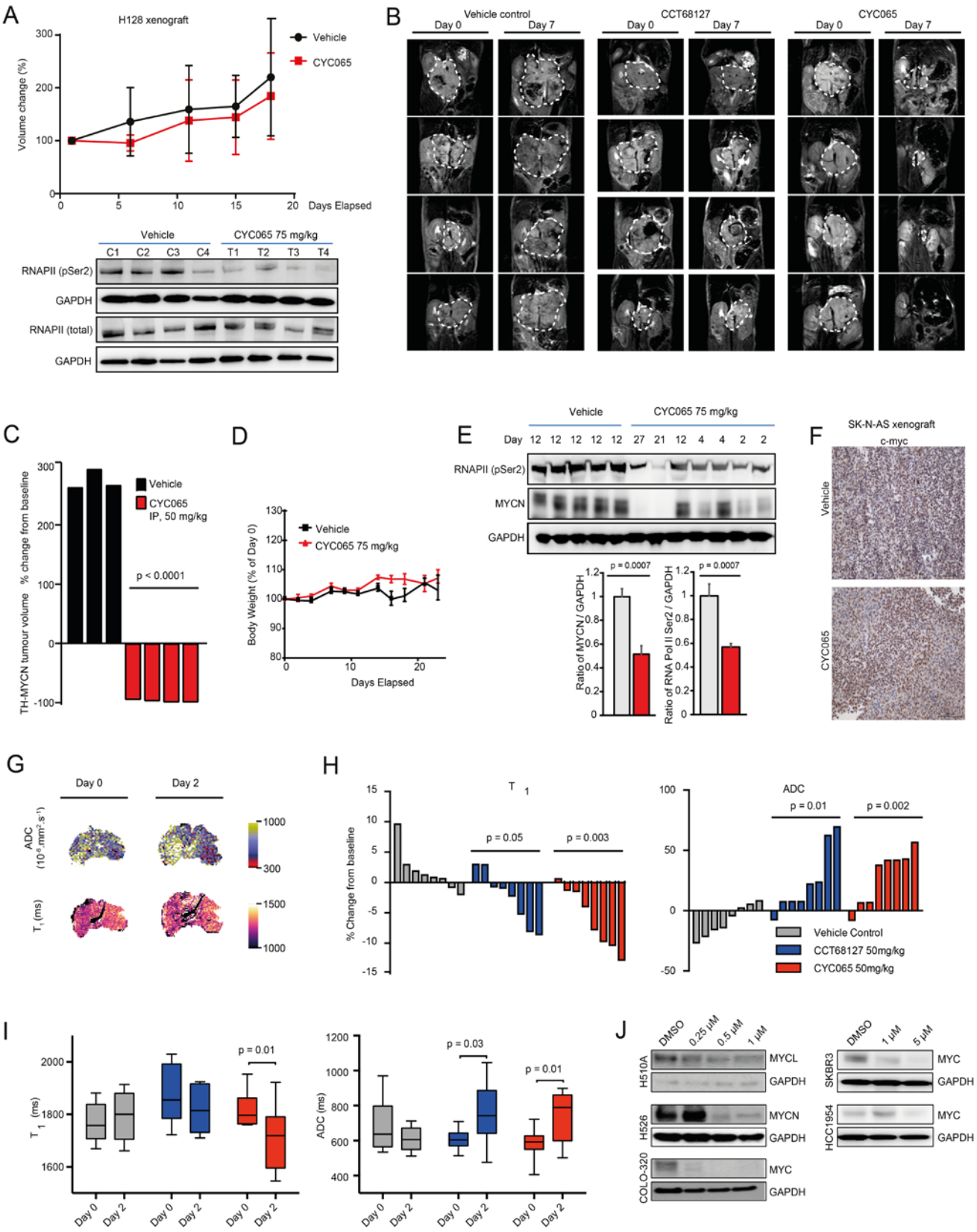

1077

Supplemental Figure 8: Molecular and non-invasive MRI biomarker of response to CYC065 in vivo.

A, Effects of CYC065 on the growth and survival of H-128 (non Myc-driven) lung xenografts in mice. Data are expressed as the mean relative tumor volumes (compared with tumor size at the start of treatment) +/- S.E.M. (n=6 vehicle, n=6 (75 mg/kg CYC065). Mice were treated in a 'five days on, two days off' schedule.

B, Coronal T_2-weighted MRI images of the abdomen of four representative tumor-bearing TH-*MYCN* mice prior to and 7 days following a 'five days on, two days off' schedule with CYC065 (50mg/kg), CCT68127 (50mg/kg) or vehicle (--- tumor).

C, Waterfall plot documenting relative changes in tumor volume in the TH-*MYCN* GEM model following seven-day treatment with 50mg/kg CYC065, ($p<0.001$) in a 'five days on, two days off' schedule. Route of administration: IP (Significance was calculated using two-tailed unpaired Student's t-test).

D, Body weights for treated and control TH-*MYCN* mice.

E, Representative Kelly xenografts harvested at the indicated time for immunoblot analysis for MYCN, p-RNAPII-Ser2 and GAPDH. Graph showing level of MYCN and p- RNAPII-Ser2 after treatment (Significance was calculated using two-tailed unpaired Student's t-test).

F, Representative SK-N-AS xenografts harvested at the end of the trial from Figure 6b for immunohistochemical analysis for c-MYC. Scale bar: 100µm.

G, Parametric functional MRI maps showing the change in the apparent diffusion coefficient (ADC) and tumor spin lattice relaxation time T_1 values 24hr after treatment with vehicle control.

H, Waterfall plot showing relative changes in median native T_1 and ADC in the TH-*MYCN* GEM model 24hr following treatment with 50mg/kg CCT68127, 50mg/kg CYC065 or vehicle. (Significance was calculated using two-tailed unpaired Student's t-test with a 5% level of significance).

I, Change in median native T_1 and ADC values prior to (D0) and 24hr (D2) after treatment with 50mg/kg CYC065 or vehicle. (Significance was calculated using two-tailed paired Student's t-test with a 5% level of significance).

J, Immunoblots showing the effects of 8hr treatment of CYC065 on MYC family members in lung (H510A and H526), colon (COLO-320) and breast (SKBR3 and HCC1954) cancer cell lines.